

Steady-state hydrodynamic instabilities of active liquid crystals: Hybrid lattice Boltzmann simulations

D. Marenduzzo¹, E. Orlandini², M.E. Cates¹, J.M. Yeomans³

¹ *SUPA, School of Physics, University of Edinburgh,
Mayfield Road, Edinburgh EH9 3JZ, Scotland*

² *Dipartimento di Fisica and Sezione INFN,
Universita' di Padova, Via Marzolo 8, 35131 Padova, Italy*

³ *The Rudolf Peierls Centre for Theoretical Physics,
1 Keble Road, Oxford OX1 3NP, England*

Abstract

We report hybrid lattice Boltzmann (HLB) simulations of the hydrodynamics of an active nematic liquid crystal sandwiched between confining walls with various anchoring conditions. We confirm the existence of a transition between a passive phase and an active phase, in which there is spontaneous flow in the steady state. This transition is attained for sufficiently “extensile” rods, in the case of flow-aligning liquid crystals, and for sufficiently “contractile” ones for flow-tumbling materials. In a quasi-1D geometry, deep in the active phase of flow-aligning materials, our simulations give evidence of hysteresis and history-dependent steady states, as well as of spontaneous banded flow. Flow-tumbling materials, in contrast, re-arrange themselves so that only the two boundary layers flow in steady state. Two-dimensional simulations, with periodic boundary conditions, show additional instabilities, with the spontaneous flow appearing as patterns made up of “convection rolls”. These results demonstrate a remarkable richness (including dependence on anchoring conditions) in the steady-state phase behaviour of active materials, even in the absence of external forcing; they have no counterpart for passive nematics. Our HLB methodology, which combines lattice Boltzmann for momentum transport with a finite difference scheme for the order parameter dynamics, offers a robust and efficient method for probing the complex hydrodynamic behaviour of active nematics.

I. INTRODUCTION

Active viscoelastic gels such as suspensions of active particles and active liquid crystals are soft materials receiving increasing theoretical and experimental attention [1, 2, 3, 4, 5, 6, 7, 8, 9, 10, 11, 12, 13, 14, 15, 16, 17, 18, 19, 20]. Such materials are called “active” [21] because they continuously burn energy, for example in the form of ATP, and this drives them out of thermodynamic equilibrium even when there is no external force. Activity imparts non-trivial physical properties. Perhaps the most striking is that spontaneous flow can exist in non-driven active materials [1, 2, 3, 4, 5, 6, 7], in sharp contrast to their passive liquid crystalline counterparts. Thus such materials, while always remaining active in a microscopic sense, can undergo a phase transition from a passive phase (where activity is macroscopically incoherent) to an active phase (exhibiting spontaneous flow).

Active materials are typically encountered in biological contexts (although non-biological counterparts may also be realized, for instance with vibrated granular rods [8]). Examples include suspensions of bacterial swimmers [1, 9, 10], cell extracts [11, 12], self-propelled colloidal particles [13], and cytoskeletal gels interacting with molecular motors, such as actomyosin solutions or microtubular networks in the presence of kinesin [14, 15, 16, 17, 18]. Activity leads to striking phenomena such as bacterial swarming, cytoplasmic streaming and elastotaxis [1]. Furthermore, many biological gels, such as actin and neurofilament networks, thicken when sheared [19]. This is the opposite of the typical behaviour of viscous polymeric fluids such as molten plastics, which flow more easily as shear stress increases. Activity has been suggested to be amongst the possible causes of this peculiar flow response [1, 20].

In this paper we present a series of hybrid lattice Boltzmann simulations of the hydrodynamic equations of motion of an active nematic liquid crystal. Derivations of the continuum equations we use are given in, e.g., Refs. [1, 3, 6] and are not repeated here. However we are aware of no numerical studies of the equations (with the exception of our previous work in [20], which is a short report using a different algorithm). These are the main focus of our work. Our model considers a varying order parameter so that defects are automatically incorporated, as is flow-induced or paranematic ordering. We show that, in the limit of a uniaxial active liquid crystal with spatially uniform and temporally constant magnitude of order parameter (we call this limiting case the “Ericksen–Leslie” model in analogy with the terminology usually adopted for passive liquid crystals), our model reduces to the equations considered in Ref. [7]. We then consider the specific case of a material that is sandwiched between two infinite parallel planes at which the director field is anchored along a given direction. We first choose the anchoring to be along one of the directions in the plane (homogeneous anchoring), and we then work out the case in which there is different (conflicting) anchoring at the two boundary plates (homogeneous at the top, and homeotropic, i.e. normal to the surface, at the bottom). When the anchoring is the same at both boundaries we find that there is a phase transition [22] between a passive and an active phase when the “activity” ζ , a parameter which measures the coupling between pressure tensor and order parameter (see Section II for details), exceeds in absolute value a finite threshold. For flow-aligning materials,

the transition occurs for sufficiently extensile rods; for tumbling materials it occurs for sufficiently contractile ones. (Here “extensile” means tending to propel fluid outwards along the long axis or molecular director \mathbf{n} , drawing it in radially on the midplane. while “contractile” means the opposite [1].) Mixed boundary conditions, instead, lead to a zero activity threshold.

For homogeneous anchoring, we compare the numerical phase boundary to the one found in Ref. [7] via a linear stability analysis, finding a good agreement. However, we show that the velocity profile found from the stability analysis is itself unstable away from the phase boundary.

We also explore the nature of the solutions of the equations of motion (director and velocity field profiles) deep in the active phase, where we find that representative flow-tumbling and flow-aligning materials behave in a vastly different manner. The former can sustain a quasi-Poiseuille or banded flow, while spontaneous flow in the latter gets increasingly confined to a region close to the boundaries.

Far from the phase boundary between the active and the passive phase there is strong hysteresis, with multistable and history-dependent solutions. These suggest that deep in the active phase the dynamics might be chaotic. It would be interesting to further explore the connections between the active nematic hydrodynamics deep in the active phase and the rheochaotic behaviour which selected passive liquid crystals display when they are subjected to an external forcing [24, 25, 26]. There may also be qualitative analogies to the weakly turbulent viscoelastic flow discussed in [27].

Finally, we consider a quasi-2D case of a thin extensile flow-aligning active liquid crystal film, wrapped on a cylindrical surface (i.e. with periodic boundary conditions). Our simulations shows that there are additional instabilities in this geometry. Spontaneous flow this time appears as convection rolls, which, deeper in the active phase, transiently increase in number and eventually split up leading to a highly distorted flowing director field pattern.

We close this introduction with some notes on nomenclature and wording. Firstly, an active gel is different from a fluid which is driven out of equilibrium by an *external* shear or heat flow, cases for which there is an important and vast literature (see e.g. [28, 29]). In an active gel the driving is *internal*, as, for instance, a bacterium uses up ATP to propel itself.

Secondly, at first glance our system shares some aspects with fluids which are driven out of equilibrium by a chemical reaction. There is a significant literature on reaction-diffusion equations which lead to pattern formation [23, 30, 31]. Ultimately, our systems are chemically driven (e.g. via ATP hydrolysis), but they differ from conventional reaction-diffusion systems in two ways. Firstly, the underlying fluid has liquid crystalline order even in the passive state. Secondly, the activity enters the equations of motion through a modification of the stress tensor in the Navier-Stokes equations by a term which is non-potential (i.e. it cannot be derived on the basis of any free energy). This makes the equations of active systems quite distinct from those addressed by reaction-diffusion models.

II. MODELS AND METHODS

A. Equations of motion

We employ a Landau-de Gennes free energy \mathcal{F} , whose density we name f , to describe the equilibrium of the active liquid crystal (LC) in its passive phase (i.e. when the activity parameters are switched off, see below). This free energy density can be written as a sum of two terms. The first is a bulk contribution,

$$f_1 = \frac{A_0}{2} \left(1 - \frac{\gamma}{3}\right) Q_{\alpha\beta}^2 - \frac{A_0\gamma}{3} Q_{\alpha\beta} Q_{\beta\gamma} Q_{\gamma\alpha} + \frac{A_0\gamma}{4} (Q_{\alpha\beta}^2)^2, \quad (1)$$

while the second is a distortion term, which we take in a (standard) one-constant approximation as [32]

$$f_2 = \frac{K}{2} (\partial_\gamma Q_{\alpha\beta})^2. \quad (2)$$

In the equations above, A_0 is a constant, γ controls the magnitude of order (it may be viewed as an effective temperature or concentration for thermotropic and lyotropic liquid crystals respectively), while K is an elastic constant. $f = f_1 + f_2$ is a standard free energy density to describe passive nematic liquid crystals [32]. Here and in what follows Greek indices denote cartesian components and summation over repeated indices is implied.

The anchoring of the director field on the boundary surfaces (Fig. 1) to a chosen director \hat{n}^0 is ensured by adding a surface term

$$f_s = \frac{1}{2} W_0 (Q_{\alpha\beta} - Q_{\alpha\beta}^0)^2 \quad (3)$$

$$Q_{\alpha\beta}^0 = S_0 (n_\alpha^0 n_\beta^0 - \delta_{\alpha\beta}/3) \quad (4)$$

The parameter W_0 controls the strength of the anchoring, while S_0 determines the degree of the surface order. If the surface order is equal to the bulk order, S_0 should be taken equal to q , the order parameter in the bulk (3/2 times the largest eigenvalue of the \mathbf{Q} tensor). W_0 is large (strong anchoring) in what follows.

The equation of motion for \mathbf{Q} is taken to be [33, 34, 35]

$$(\partial_t + \vec{u} \cdot \nabla) \mathbf{Q} - \mathbf{S}(\mathbf{W}, \mathbf{Q}) = \Gamma \mathbf{H} + \lambda \mathbf{Q} \quad (5)$$

where Γ is a collective rotational diffusion constant, and λ is an activity parameter of the liquid crystalline gel. The form of Eq. 5 was suggested on the basis of symmetry in Refs. [1, 3] and derived starting from an underlying microscopic model in Ref. [6]. The first term on the left-hand side of Eq. (5) is the material derivative describing the usual time dependence of a quantity advected by a fluid with velocity \vec{u} . This is generalized for rod-like molecules by a second term

$$\begin{aligned} \mathbf{S}(\mathbf{W}, \mathbf{Q}) &= (\xi \mathbf{D} + \omega)(\mathbf{Q} + \mathbf{I}/3) + (\mathbf{Q} + \mathbf{I}/3)(\xi \mathbf{D} - \omega) \\ &\quad - 2\xi(\mathbf{Q} + \mathbf{I}/3)\text{Tr}(\mathbf{Q}\mathbf{W}) \end{aligned} \quad (6)$$

where Tr denotes the tensorial trace, while $\mathbf{D} = (\mathbf{W} + \mathbf{W}^T)/2$ and $\boldsymbol{\omega} = (\mathbf{W} - \mathbf{W}^T)/2$ are the symmetric part and the anti-symmetric part respectively of the velocity gradient tensor $W_{\alpha\beta} = \partial_\beta u_\alpha$. The constant ξ depends on the molecular details of a given liquid crystal. The first term on the right-hand side of Eq. (5) describes the relaxation of the order parameter towards the minimum of the free energy. The molecular field \mathbf{H} which provides the force for this motion is given by

$$\mathbf{H} = -\frac{\delta\mathcal{F}}{\delta\mathbf{Q}} + (\mathbf{I}/3)\text{Tr}\frac{\delta\mathcal{F}}{\delta\mathbf{Q}}. \quad (7)$$

The fluid velocity, \vec{u} , obeys the continuity equation and the Navier-Stokes equation,

$$\rho(\partial_t + u_\beta\partial_\beta)u_\alpha = \partial_\beta(\Pi_{\alpha\beta}) + \eta\partial_\beta(\partial_\alpha u_\beta + \partial_\beta u_\alpha) \quad (8)$$

where ρ is the fluid density, η is an isotropic viscosity, $\Pi_{\alpha\beta} = \Pi_{\alpha\beta}^{\text{passive}} + \Pi_{\alpha\beta}^{\text{active}}$, and we have neglected an extra term proportional to $\partial_\alpha u_\alpha$ which is zero in the case we are interested in (incompressible fluids). The stress tensor $\Pi_{\alpha\beta}^{\text{passive}}$ necessary to describe ordinary LC hydrodynamics is:

$$\begin{aligned} \Pi_{\alpha\beta}^{\text{passive}} = & -P_0\delta_{\alpha\beta} + 2\xi(Q_{\alpha\beta} + \frac{1}{3}\delta_{\alpha\beta})Q_{\gamma\epsilon}H_{\gamma\epsilon} \\ & -\xi H_{\alpha\gamma}(Q_{\gamma\beta} + \frac{1}{3}\delta_{\gamma\beta}) - \xi(Q_{\alpha\gamma} + \frac{1}{3}\delta_{\alpha\gamma})H_{\gamma\beta} \\ & -\partial_\alpha Q_{\gamma\nu}\frac{\delta\mathcal{F}}{\delta\partial_\beta Q_{\gamma\nu}} + Q_{\alpha\gamma}H_{\gamma\beta} - H_{\alpha\gamma}Q_{\gamma\beta} \\ \equiv & \sigma_{\alpha\beta} + \tau_{\alpha\beta} - \partial_\alpha Q_{\gamma\nu}\frac{\delta\mathcal{F}}{\delta\partial_\beta Q_{\gamma\nu}}. \end{aligned} \quad (9)$$

In Eq. (9) we have defined the symmetric and anti-symmetric part of the passive stress tensor (not including the double gradient term $\partial_\alpha Q_{\gamma\nu}\frac{\delta\mathcal{F}}{\delta\partial_\beta Q_{\gamma\nu}}$) as $\sigma_{\alpha\beta}$ and $\tau_{\alpha\beta}$ respectively, for later convenience. P_0 is a constant in the simulations reported here. The active term is given by

$$\Pi_{\alpha\beta}^{\text{active}} = -\zeta Q_{\alpha\beta} \quad (10)$$

where ζ is a second activity constant [1, 7]. Note that with the sign convention chosen here $\zeta > 0$ corresponds to extensile rods and $\zeta < 0$ to contractile ones [1]. As for Eq. 5, the explicit form of the active contribution to the stress tensor entering Eq. 8 was proposed on the basis of a symmetry analysis of a fluid of contractile or extensile dipolar objects in [1]. It was also derived by coarse graining a more microscopic model for a solution of actin fibers and myosins in Ref. [6].

A full understanding of the physical origin (in both bacterial suspensions and actomyosin gels) of the phenomenological couplings ζ and λ , as well as of the range of values these may attain in physically relevant situations, will require multi-scale modelling at different coarse graining levels, and more accurate quantitative experiments. These are at the moment still lacking. However, we already know from experiments and from some more microscopic approaches, that actomyosin gels are contractile, so that in physiological conditions those materials should be described by negative values of ζ [36]. The term proportional to λ has been proposed in Ref. [1] as a symmetry

allowed term which, for dilute bacterial suspensions, should be negative and proportional to the inverse of the time scale for relaxation of activity-induced ordering. In Ref. [7] it was pointed out that, instead, $\lambda > 0$ when describing concentrated actomyosin gels and other systems which display zipping or other self-alignment effects (this is relevant for the cases considered in [37]).

It is important to note that the model we have just written down reduces for $\lambda = \zeta = 0$ to the Beris-Edwards model for LC hydrodynamics. For a sample of uniaxial active LCs with a spatially uniform degree of orientational order, the director field (also called polarisation field in Refs. [3, 4, 5]) \vec{n} is defined through

$$Q_{\alpha\beta} = q (n_\alpha n_\beta - \delta_{\alpha\beta}/3), \quad (11)$$

where q is the degree of ordering in the system (assumed to be spatially uniform). In this limit our model can be shown to reduce to the vectorial model considered in [3, 5], as will be shown explicitly in Section III.

B. Hybrid lattice Boltzmann algorithm

The differential equations (5) and (8) may both be solved by using a lattice Boltzmann (LB) algorithm [38], based on the 3-dimensional lattice Boltzmann algorithm for conventional liquid crystals [40], generalised to include the two extra active terms, as we discussed in Ref. [20].

Here we use a different route, and solve Eq. (5) via a finite difference predictor-corrector algorithm, while lattice Boltzmann is used to solve the Navier-Stokes equation, (8). With respect to a full LB approach [39, 40], the primary advantage of this method is that it will allow simulations of larger systems as it involves consistently smaller memory requirements. Indeed, while in a full LB treatment one has to store 6 sets of 15 distribution functions at any lattice point (if we choose the 3DQ15 velocity vector lattice [38] as we do here), just one set of distribution functions plus the five independent components of the \mathbf{Q} tensor, is needed in this hybrid algorithm. Furthermore, we avoid in this way the error term arising in the Chapman-Enskog expansion used to connect the LB model to the order parameter evolution equation in the continuum limit [39].

Lattice Boltzmann algorithms to solve the Navier-Stokes equations of a simple fluid are defined in terms of a single set of partial distribution functions, the scalars $f_i(\vec{x})$, that sum on each lattice site \vec{x} to give the density. Each f_i is associated with a lattice vector \vec{e}_i [40]. We choose a 15-velocity model on the cubic lattice with lattice vectors:

$$\vec{e}_i^{(0)} = (0, 0, 0) \quad (12)$$

$$\vec{e}_i^{(1)} = (\pm 1, 0, 0), (0, \pm 1, 0), (0, 0, \pm 1) \quad (13)$$

$$\vec{e}_i^{(2)} = (\pm 1, \pm 1, \pm 1). \quad (14)$$

The indices, i , are ordered so that $i = 0$ corresponds to $\vec{e}_i^{(0)}$, $i = 1, \dots, 6$ correspond to the $\vec{e}_i^{(1)}$ set and $i = 7, \dots, 14$ to the $\vec{e}_i^{(2)}$ set. For our hybrid code, the input to the equilibrium distribution

functions has to come from the solution (via finite difference methods) of the coupled Eq. (5). This differs from the fully LB treatment of nematics; see Refs. [39, 40].

Physical variables are defined as moments of the distribution functions:

$$\rho = \sum_i f_i, \quad \rho u_\alpha = \sum_i f_i e_{i\alpha}. \quad (15)$$

The distribution functions evolve in a time step Δt according to

$$f_i(\vec{x} + \vec{e}_i \Delta t, t + \Delta t) - f_i(\vec{x}, t) = \frac{\Delta t}{2} [\mathcal{C}_{f_i}(\vec{x}, t, \{f_i\}) + \mathcal{C}_{f_i}(\vec{x} + \vec{e}_i \Delta t, t + \Delta t, \{f_i^*\})]. \quad (16)$$

This represents free streaming with velocity \vec{e}_i followed by a collision step which allows the distributions to relax towards equilibrium. The f_i^* 's are first order approximations to $f_i(\vec{x} + \vec{e}_i \Delta t, t + \Delta t)$, and they are obtained by using $\Delta t \mathcal{C}_{f_i}(\vec{x}, t, \{f_i\})$ on the right hand side of Eq. (16). Discretizing in this way, which is similar to a predictor-corrector scheme, has the advantages that lattice viscosity terms are eliminated to second order and that the stability of the scheme is improved [39].

The collision operators are taken to have the form of a single relaxation time Boltzmann equation, together with a forcing term

$$\mathcal{C}_{f_i}(\vec{x}, t, \{f_i\}) = -\frac{1}{\tau_f} (f_i(\vec{x}, t) - f_i^{eq}(\vec{x}, t, \{f_i\})) + p_i(\vec{x}, t, \{f_i\}), \quad (17)$$

The form of the equations of motion follow from the choice of the moments of the equilibrium distributions f_i^{eq} and the driving terms p_i . Moreover, f_i^{eq} is constrained by

$$\sum_i f_i^{eq} = \rho, \quad \sum_i f_i^{eq} e_{i\alpha} = \rho u_\alpha, \quad \sum_i f_i^{eq} e_{i\alpha} e_{i\beta} = -\sigma_{\alpha\beta} + \rho u_\alpha u_\beta \quad (18)$$

where the zeroth and first moments are chosen to impose conservation of mass and momentum. The second moment of f^{eq} is determined by $\sigma_{\alpha\beta}$, whereas the divergences of $\tau_{\alpha\beta}$ and of $\partial_\alpha Q_{\gamma\nu} \frac{\delta \mathcal{F}}{\delta \partial_\beta Q_{\gamma\nu}}$ enter effectively as a body force:

$$\sum_i p_i = 0, \quad \sum_i p_i e_{i\alpha} = \partial_\beta \tau_{\alpha\beta} - \partial_\beta \left(\partial_\alpha Q_{\gamma\nu} \frac{\delta \mathcal{F}}{\delta \partial_\beta Q_{\gamma\nu}} \right), \quad \sum_i p_i e_{i\alpha} e_{i\beta} = 0. \quad (19)$$

Conditions (18)–(19) are satisfied by writing the equilibrium distribution functions and forcing terms as polynomial expansions in the velocity. The coefficients in the expansion are (in general non-uniquely) determined by the requirements that these constraints are fulfilled (see Ref. [40] for details). The active contributions then simply alter the constraints on the second moment of the f_i 's. (Alternatively the derivative of the active term could be entered as a body force and thus would modify the constraint on the first moment of the p_i 's; we do not pursue this here.)

In Appendix (A) we give a quantitative comparison between the hybrid LB algorithm used here and two versions of a fully LB-based code for active nematics [20]. The hybrid code is quite satisfactory in performance; it is also easier to code and runs substantially faster due to the elimination of the cumbersome additional distribution functions required to represent the order parameter dynamics within a fully LB-based approach.

III. MAPPING TO ERICKSEN-LESLIE LEVEL EQUATIONS

In this section, we consider the limit of the equations of motion (5) and (8) when the active molecules are uniaxial, so that the order parameter can be written in the form $Q_{\alpha\beta} = q(n_\alpha n_\beta - \delta_{\alpha\beta}/3)$ (\vec{n} being the usual nematic director field). We furthermore assume that the magnitude q of the nematic ordering is independent of space and time. The resulting simplified theory is commonly employed in the physics of active gels (see e.g. Ref. [3, 5]); using it, some analytical results have been found. It is thus useful to explicitly consider this limit (i) to show that our equations map onto those of Ref. [5, 7] for uniaxial systems, and (ii) to quantitatively check our numerical results against those found analytically for the phase boundaries separating the active and passive states [7]. In this Section quantities labelled by ‘‘EL’’ refer to the resulting director-field model, which is the direct counterpart of the Ericksen-Leslie theory [32] of passive liquid crystal hydrodynamics.

A. Order parameter equation of motion

We first note that the evolution equation (5) of the tensor order parameter can be written in the usual form for a purely passive system

$$(\partial_t + \vec{u} \cdot \nabla) \mathbf{Q} - \mathbf{S}(\mathbf{W}, \mathbf{Q}) = \Gamma \mathbf{H}' \quad (20)$$

so long as we write an effective molecular field

$$\mathbf{H}' = \mathbf{H} + \frac{\lambda}{\Gamma} \mathbf{Q} \quad (21)$$

This implies that the the classical linear (in \mathbf{Q}) term of the molecular field, namely

$$-A_0(1 - \gamma/3) Q_{\alpha\beta}, \quad (22)$$

is now effectively replaced by

$$\left(-A_0(1 - \gamma/3) + \frac{\lambda}{\Gamma} \right) Q_{\alpha\beta}. \quad (23)$$

In this manner the ‘‘equilibrium’’ properties of active nematics can be said to differ from the passive ones because of the presence of the active parameter λ . (This contrasts with the role of ζ , which has no equilibrium counterpart. We will see below, moreover, that the shift created by λ has no dynamical consequences in systems where the ordering strength q is fixed.)

After some straightforward algebra (see e.g. [33] and Refs. therein), one finds that the linear term now changes sign for $\gamma = \gamma^*$, with

$$\gamma^* = 3 \left(1 - \frac{\lambda}{\Gamma A_0} \right). \quad (24)$$

Similarly the transition point $\gamma = \gamma_c$ for the first-order isotropic-to-nematic transition obeys

$$\gamma_c(\lambda) = \frac{27}{10} \left(1 - \frac{\lambda}{\Gamma A_0} \right) = \gamma_c(0) \left(1 - \frac{\lambda}{\Gamma A_0} \right). \quad (25)$$

Furthermore, for uniaxial nematics with a spatially uniform degree of ordering q (as assumed at Ericksen-Leslie level – see above), the solution for q becomes

$$q(\lambda) = \frac{1}{4} + \frac{3}{4} \sqrt{1 - \frac{8}{3\gamma} + \frac{8}{3\gamma} \frac{\lambda}{\Gamma A_0}}. \quad (26)$$

(Note that this is 3/2 times the largest eigenvalue of the \mathbf{Q} tensor.)

The conventional passive case is recovered by setting $\lambda = 0$ in equations (23–26). Note that the value of q at the transition, $q_c = 1/3$, is independent of λ since it is insensitive to the quadratic term of the free energy density. However, the condition for real solutions (positivity of the term inside the square root) for active nematics is shifted by nonzero λ and becomes

$$\bar{\gamma} = \frac{8}{3} \left(1 - \frac{\lambda}{\Gamma A_0} \right). \quad (27)$$

The dynamics of the director field in a uniaxial active liquid crystal of fixed q is controlled by three parameters. These are γ_{EL} , the liquid crystal rotational viscosity; ν_{EL} , which is another viscosity determining whether the liquid crystal (in its passive phase) is flow-aligning or flow-tumbling (for $|\nu_{EL}|$ larger and smaller than 1 respectively); and λ_{EL} , which determines the magnitude of activity-induced ordering. It is possible to map the dynamical equation of motion for $Q_{\alpha\beta}$ (20) onto the model considered in Ref. [7] (the details are worked out in Appendix B), which leads to the following identifications:

$$\gamma_{EL} = \gamma_1 = \frac{2q^2}{\Gamma}, \quad (28)$$

$$\nu_{EL} = \frac{\gamma_2}{\gamma_1} = -\frac{(q+2)\xi}{3q}, \quad (29)$$

$$\lambda_{EL} = 0. \quad (30)$$

These relations show that in our model the dynamics of the tensorial order parameter may be controlled by tuning ξ and Γ . Furthermore, we note that our parameter λ does not control λ_{EL} directly, because in Ref. [7] this parameter can already be adsorbed into a Lagrange multiplier introduced to maintain fixed q . (To emphasize this, we set it to zero above; see also Appendix B.) However, changing λ in our equations does alter q , so qualitatively the meaning of this parameter is similar to that of λ_{EL} in [7] insofar as it determines the strength of activity-induced self-alignment effects. The relations (28), (29), give rise to a non-trivial dependence of the parameter ν_{EL} on γ and ξ as shown in figure 1.

B. Navier-Stokes equation

We now map out the parameters entering the Navier-Stokes equation (8) onto the analogous equation derived at director-field level in Ref. [7], which is written in terms of the ‘‘vectorial’’ molecular field h_μ and of the director field, n_μ . In Ref. [7], the velocity field at steady state of an active gel is determined by ν_{EL} (see Sec.C), η_{EL} , which is an isotropic viscosity similar to the one introduced in Eq. (8), and ζ_{EL} , which controls the hydrodynamics in the active phase, determining whether the active liquid crystal is extensile or contractile as discussed in Section II. (Note that ζ_{EL} controls the effect of activity on the Navier-Stokes sector, but does not enter directly the order parameter dynamics as set up in Sec.C.)

After some algebra (the details of which are worked out in Appendix B), we can rewrite Eq.(8) in the required limit of uniaxiality and fixed q . We find that the six Leslie viscosities for a purely passive liquid crystal ($\lambda = \zeta = 0$), which are usually called $\alpha_{1,\dots,6}$ [32], are:

$$\alpha_1 = -\frac{2}{3\Gamma}q^2(3 + 4q - 4q^2)\xi^2, \quad (31)$$

$$\alpha_2 = \frac{1}{\Gamma}\left(-\frac{1}{3}q(2 + q)\xi - q^2\right), \quad (32)$$

$$\alpha_3 = \frac{1}{\Gamma}\left(-\frac{1}{3}q(2 + q)\xi + q^2\right), \quad (33)$$

$$\alpha_4 = \frac{4}{9\Gamma}(1 - q)^2\xi^2 + \eta, \quad (34)$$

$$\alpha_5 = \frac{1}{3\Gamma}(q(4 - q)\xi^2 + q(2 + q)\xi), \quad (35)$$

$$\alpha_6 = \frac{1}{3\Gamma}(q(4 - q)\xi^2 - q(2 + q)\xi). \quad (36)$$

The Parodi relations,

$$\alpha_3 - \alpha_2 = \frac{2q^2}{\Gamma} = \gamma_1, \quad (37)$$

$$\alpha_6 - \alpha_5 = -\frac{2}{3}q\xi\left(\frac{q + 2}{\Gamma}\right) = \gamma_2, \quad (38)$$

$$\alpha_2 + \alpha_3 = \alpha_6 - \alpha_5, \quad (39)$$

are easily seen to hold. The Ericksen-Leslie level viscosity and active stress term are recovered as:

$$\eta_{EL} = \eta + \frac{2}{9\Gamma}(q - 1)^2\xi^2, \quad (40)$$

$$\zeta_{EL} = \zeta. \quad (41)$$

Using the above relations and the results of Ref. [7], we obtain the phase boundary in the (ζ, λ) plane, for an active nematic confined between parallel plates at separation L , with homogenous anchoring at the walls (Fig.3):

$$\zeta L^2 = \frac{12\pi^2 K (12 \tau_f \Gamma - 5 \xi q^2 - 14 \xi q + \xi + \xi^2 q^2 + 4 \xi^2 + 4 \xi^2 q + 9 q^2)}{9 (\xi q + 2 \xi - 3 q)}. \quad (42)$$

From Eq. (42) it is apparent that the critical activity threshold beyond which spontaneous flow is found scales like L^{-2} , and thus vanishes for an infinite system. Note that the dependence on λ of the phase boundary is indirect, via q . Fig. 2 shows an example of comparison between analytical and simulated phase boundary, from which it is apparent that there is a good agreement.

IV. RESULTS

Most of the results which we present below refer to a quasi-1D system in which the active nematic is sandwiched between two plates at separation L in the z direction, with translational invariance assumed in x and y (Fig. 3). We consider two different boundary conditions: either homogeneous anchoring along the y -direction, or mixed (conflicting) anchoring at the two plates. We will also refer to the angle between the director field and the positive y direction as the polarization angle, θ , the convention being that $\theta > 0$ if the positive y axis can be superimposed with the director field with an anti-clockwise rotation of an angle $|\theta|$ (which is defined to be smaller than π), around the x axis.

A. Spontaneous flow transition in Freedericksz cells

We first consider homogeneous anchoring where the polarization at the confining surface is parallel to the y -direction, $\theta = 0$. (This geometry is known as the Freedericksz cell in passive liquid crystal device terminology, [32].) By considering Eq. 26 we see that the order parameter q remains between 0 and 1 for small values of λ . Furthermore, we note that for $\xi = 0.7$ and $\xi = 0.5$ the system is respectively in the flow-aligning regime (point A in Fig. 1) and in the flow-tumbling regime (point B). Let us first concentrate on the flow-aligning regime (point A). For definiteness we now fix $\lambda = 0$, $\tau_f = 2.5$, $A_0 = 0.1$, $K = 0.04$, $\Gamma \sim 0.34$ and $\gamma = 3$; while ξ can take on the discrete values 0.5, 0.7 as just described, and L and ζ are variable. Note that, as described previously, setting $\lambda = 0$ eliminates the shift in q arising from self-alignment but this term can anyway be adsorbed into an effective (quasi-passive) free energy. Accordingly, the important activity parameter, for our purposes, is simply ζ .

1. Flow-aligning regime

For $\xi = 0.7$, the system is flow-aligning and, for instance with $\zeta = 0.005$, the active LC is extensile. In Figure 4 we show the time evolution of the components n_y, n_z of the polarization vector at the center of a system of size $L = 100$ lattice units (n_x is identically zero in this case). The polarisation field was initialized along the y direction except for the midpoint director field, which was initialised with $\theta = 10^\circ$. As one can see for $t > t^* \sim 10^5$ timesteps, the system undergoes a transition to an active state, characterised by a spontaneous flow.

This happens when the scaling variable ζL^2 becomes larger than the critical value found through the solution of Eq. 42. Thus there are two ways of entering the active phase: either by increasing the value of ζ at fixed L , or by increasing the system size at fixed activity. In Figs. 5 and 6 we explore the system behaviour (respectively director and flow field at steady state) when the active phase is entered via an increase in the activity parameter ζ .

By means of a stability analysis, valid very close to the phase boundary, an analytic expression for $u_y(z)$ was found in [7]. This predicts a sinusoidal modulation with a node at the centre of the channel. While our numerics shows this solution to be metastable for a long time close to the threshold, the eventual steady state we find is a quasi-Poiseuille flow with a maximum flow velocity, not a nodal point, at the centre of the channel (Fig. 5). Thus with homogeneous boundary conditions and assumed translational invariance along the flow direction, we obtain a spontaneous net mass flux rather than the balancing fluxes of forward and backward fluid in the two halves of the cell, suggested by the analysis of [7]. Our numerical simulations thus suggest that the perturbative solution is stable at most within a very narrow region close to the phase boundary. The overall mass flux is set in a direction chosen by spontaneous symmetry breaking or, in practice, small deviations from symmetry between y and $-y$ in the initial condition. Note that for a fixed initial condition as selected above, the flow direction can also switch on variation in ζ : to ease comparisons, some such switches are silently reversed in the figures presented here and below.

Upon increasing the value of ζL^2 (i.e. moving deeper inside the active phase) the flow pattern changes from quasi-Poiseuille flow to a “banded” flow, with regions of rather well defined and distinct local shear rates (Fig. 6). These *bands* (which are clearer and more numerous in larger samples, see Fig. 7) correspond to regions of aligned liquid crystal, which are separated by sharp interfaces. As the equations deep in the active phase are strongly non-linear, no analytical results so far exist to probe the behaviour of an active gel in this regime. The utility of a robust numerical algorithm, as we have developed here with our HLB code, is highly apparent when addressing the potentially complex behaviour in such regimes. The model we consider allows for a non-constant value of the order parameter q and we can thus quantify the variations in q that are neglected in a director field model. Variations in q are at most of 1 – 5% in the simulations reported above, and small dips in the order parameter correspond to the spatially rapidly varying regions in the director field profile (i.e. in the “kinks” which appear at the band edges). Furthermore, these small changes are only encountered far from the phase boundary.

2. Flow-tumbling regime

We now turn our attention to the flow tumbling regime by considering $\xi = 0.5$, $\gamma = 3$ and $\lambda = 0$. In this case Eq. (42) suggests that, in order to have a spontaneous flow, ζ must be negative (i.e. the LC has to be contractile). This is confirmed by our simulations. We consider the value $\zeta = -0.0025$, which is just in the active phase (see Eq. (42)). In Figure 8 we show the time evolution of the components n_y, n_z of the polarization vector at the center of a system of

size $L = 100$, initialized as for the flow aligning case. As in the flow-aligning case, for $t > t^*$ the system undergoes a spontaneous alignment with a consequent spontaneous flow. The time behavior is however quite different from the one observed in the flow aligning case. In particular at $t = t^*$ the polarization vector has an abrupt variation of $\pi/2$ and then reaches a stationary value with a polarization angle which strongly deviates from the starting configuration.

As with the flow-aligning case, we can estimate the critical value ζ_c at fixed L (or L_c at a given ζ) above which the system starts to display spontaneous flow in steady state. Again as in the flow-aligning case we find good agreement between the value of the threshold estimated numerically and the analytical prediction of Eq. (42). However, a comparison between the stationary profile of velocity and polarization angle profile in the flow-aligning regime and in the flow-tumbling one (Figs. 5 and 9 respectively) shows a striking difference. While the velocity profile has the shape of a spontaneous Poiseuille flow for a flow-aligning active liquid crystal, it is zero in the centre of the channel and confined to the boundaries in the flow-tumbling case. Also the polarization angle is quite different: in the flow-aligning case the director field splays and bends so that the polarization angle approaches the Leslie values (selected by the local shear), while it is almost constant throughout the sample in the flow-tumbling case.

Upon moving deeper inside the active phase, first the velocity field becomes confined more and more to the boundaries, while the polarisation angle becomes increasingly close to 90° throughout (Fig. 9). For still larger values of the activity parameter ζ (Fig. 10), the flow changes sign, passing through an intermediate state with plug-like flow in which the polarization has the shape of a kink (notice however that $\theta = \pm 90^\circ$ are equivalent due to the head-tail symmetry of the director field). As in the flow-aligning case, order parameter variations are limited for ζ just larger (in absolute value) than the critical value. For the simulations presented here and deep in the active phase, the order parameter shows some drops (similar in magnitude to those found with flow-aligning materials) close to the boundary plates, where the shear rates are maximal.

3. *Multi-stability in the active phase*

It is important to consider whether the solutions we have found are unique (modulo the trivial bistability associated with sign-reversal, discussed above), or whether each of them is one of many possible solutions of the equations of motion with given anchoring conditions at the boundary. The selection between such solutions, if they exist, is presumably governed by the initial conditions. We focus here, for definiteness, on the case of contractile active tumbling liquid crystals.

Figs. 11 and 12 show the results of two different initial conditions on the steady state director and velocity profiles. Fig. 11 shows data for a modest value of the activity ($\sim 50\%$ larger in absolute value than the critical value to enter the active phase). It can be seen that one of the solutions has a non-zero component of the director field along the x direction, so that the director tilts out of the “shear plane” (the yz plane in Fig. 3). Fig. 12 shows another example, deeper in the active phase, in which the polarisation profiles again differ in steady state for the two different

initial conditions. One of these initial conditions is the same as above, for the other we started the director field along the z direction apart from (the boundary and) the midplane in which the polarisation angle was tilted.

Extensile aligning liquid crystals behave in a similar way. As a rule of thumb, multistability appears to increase for *intermediate* values of the activity. For the cases considered here, we only find a single (bistable) solution in the active phase close to the phase boundary and again for very large activity. It should be noted that also passive liquid crystals can have metastable multiple solution in equilibrium (for instance super-twisted structure are metastable). However, in that case (in the presence of thermal noise, and in the absence of external driving) one can speak of a “most stable solution” which is unambiguously determined by free energy minimization. No such criterion exists for our non-equilibrium problem, as the equations of motion cannot be written down completely in terms of a free energy. (Note however that, were $\zeta = 0$, this could be done even in the presence of the active self-alignment term λ .)

B. Spontaneous flow in hybrid aligned nematic cells

Now we consider a hybrid-aligned nematic cell (HAN cell, in passive liquid crystal terminology [41]), in which the polarization vector is anchored homogeneously at $z = 0$ and homeotropically at $z = L$. We restrict attention to $\xi = 0.7$, the flow-aligning case.

Unlike the Freedericksz cell, the conflicting anchoring now leads to an elastic distortion in equilibrium even within the passive phase of the active system (as it would in a strictly passive nematic). As a result *any* non-zero value of ζ , whether positive or negative, leads to spontaneous flow in steady state, as the active pressure tensor is no longer divergence-free when $\zeta \neq 0$. Thus even contractile aligning liquid crystals flow spontaneously in this geometry (Fig. 13). The velocity profiles in steady state in this case show extended regions with very low shear rate and plug-like flow, coexisting with strongly sheared “boundary layers”. This is similar to what was observed in Section IV A.1 for contractile (tumbling) liquid crystals in a Freedericksz cell geometry. The region of the cell in which the director field is close to homeotropic anchoring ($\theta = 0$) increases with $|\zeta|$.

The behaviour of extensile aligning materials in a HAN geometry is reported in Figs. 14 and 15 for smaller and larger values of ζ respectively. The spontaneous flow is asymmetric. Initially there are oppositely flowing slabs of liquid crystals, which distort the director field by creating homogeneously aligned region separated by thin regions of homeotropic ordering. These profiles are then supplanted by an asymmetric quasi-Poiseuille flow, which resembles the response of a purely passive HAN cell to a pressure difference driven flow [41]. At larger values of ζ the director profile throughout is close to the one obtained for a Freedericksz cell, with only a highly distorted boundary layer to satisfy the homeotropic anchoring at the top plane ($z = L$).

C. Spontaneous flow in two dimensions

Thus far, all simulations reported here were performed in a quasi-1D geometry, where translational invariance is assumed along x and y . The same simplification is often employed in numerical studies of passive liquid crystals (see many examples in Ref. [32], as well as e.g. Refs. [25, 41] for rheological studies); moreover, as shown above they allowed us to check detailed analytical predictions (calculated at director-field or EL level) in exactly this geometry [7]. It is clearly important and interesting to consider whether there are additional spontaneous flow instabilities in a higher dimensionality. With periodic boundary conditions such instabilities must spontaneously break the translational invariance in x and y ; we limit our attention to this case, but note that confining cell walls might also play an important role.

We next present 2D simulations ($L_z = 100, L_y = 100, L_x = 0$) in which we again have two parallel plates, normal to z ; translational invariance along x is maintained but periodic boundary conditions are used to allow breakdown of this along the flow direction, y . We initialised the simulation with the director field along the y direction except for points along the mid-plane $z = L/2$, in which there was an alternating tilt of $\pm 10^\circ$ in stripes (the width of the initial stripes did not affect the steady state reached at the end of the simulations).

Fig. 16 shows results for a moderate value of the activity parameter ζ (0.001), for which the liquid crystal enters the spontaneously flowing active phase. Spontaneous flow appears as a pair of convection rolls which lead to a splay-bend in-plane deformation of the director field profile. The order parameter is to a good approximation constant ($q \simeq 0.5$) throughout the sample. The threshold at which the spontaneous flow appears is smaller than the one found in the quasi-1D simulation (for which with the same parameters $\zeta_c \simeq 0.002$, see above). This is due to the fact that along y effectively homeotropic anchoring conditions are seen, and the active phase is entered for a smaller value of ζ in this geometry. Note that, since at onset of the convection rolls there are exactly two of these in the periodic cell, the details of the transition may now depend sensitively on the aspect ratio of the cell.

As we go deeper into the active phase, the number of convection rolls is, at early times in the simulations, larger (Fig. 17 (a1,b1)). These convection rolls then split up, and the flow field acquires an out-of-plane component (i.e. there is flow along the x direction). After this happens, a number of vortices form which lead to a complicated flow which is accompanied by the formation of defects (of topological strength $\pm 1/2$) in the director field profile. The simulation, followed in Fig. 17, does not lead to a steady state. It would seem plausible that the corresponding trajectories in phase space may be chaotic, but we have not attempted to test this directly. Moreover, once a nonzero x velocity has been acquired, there is a strong possibility of breakdown of translational invariance in x ; to explore this would require fully 3D simulations. Note however that in this regime the structural length scale of the flow appears small on the scale of the simulation cell and therefore might cease to be sensitive to its shape.

V. DISCUSSION AND CONCLUSIONS

We have presented a hybrid lattice Boltzmann algorithm to solve the equations of motion of an active nematic liquid crystal. In our equations the orientational degrees of freedom are characterised by a tensorial order parameter. This renders our algorithm general enough to deal – in principle – with non-homogeneous, flow-induced or paranematic ordering, as well as with topological defects. The model we analyse is equivalent to the one proposed in Ref. [1].

Our main results are the following. First, we have explicitly mapped our model onto the one considered in Ref. [7] in the limiting case of a uniaxial liquid crystal with a spatially uniform and time independent magnitude of ordering. This is useful when comparing the different approaches which are now being proposed to study the physics of active materials.

Second, we found a spontaneously flowing phase (active phase) for a wide range of values for the activity parameter ζ in a quasi-1D geometry where the director field is constrained to lie along a common direction along both confining plates. (A second activity parameter, λ , merely renormalizes the equilibrium parameters of the passive material.) Our simulations confirm the location of the phase transition from passive to active phase found via a linear stability analysis in Ref. [7], but show that, for a wide range of parameters within the active phase, even very close to the boundary, the spontaneous flow profile has a quite different symmetry from the one predicted by that analysis. Instead of a sinusoidal flow with a node at the midplane, flow-aligning and flow-tumbling liquid crystals display a quasi-Poiseuille flow and a “boundary layer” type flow respectively. (Both flow profiles are bistable.)

Our numerical method can readily probe, for the first time, the hydrodynamic behaviour of active materials deep in the active phase, where we gave evidence of a spontaneously banded flow for the flow-aligning case. Far from the phase boundary, there are multiple (initial condition dependent) solutions, and the system displays hysteresis.

Third, if conflicting (HAN-type) anchoring conditions are applied at the confining plates, spontaneous flow occurs for any values of the activity parameter ζ , however small. Finally, we performed two-dimensional simulations, with periodic boundary conditions along the y direction and planar anchoring along that direction on both confining plates. These suggest that there are additional instabilities in a quasi-2D geometry. Moreover, at high activity levels, there can also be a spontaneous flow also in the x direction in this geometry.

These results demonstrate a remarkable richness in the steady-state hydrodynamic behaviour of active nematic materials, even in the absence of external drive such as an imposed shear flow. (As such, they have no counterpart in the physics of passive nematics.) Our hybrid lattice Boltzmann methodology, which combines LB for momentum with finite difference methods for the order parameter tensor $Q_{\alpha\beta}$, offers a robust and efficient method for probing these effects. It can equally well handle transient phenomena, some of which we explored above, and can readily be modified to allow for imposed flow.

Our algorithm can be generalized in several ways. For instance, an additional order parameter equation, describing the time evolution of a polar vector field, can be considered with little more

effort. This would allow a full 2D study of polar active nematics [6] with a variable degree of ordering. Similarly, chiral active liquid crystals can be straightforwardly treated [42], for instance to model concentrated actomyosin solutions. Actin fibers in very concentrated solutions undergo a nematic to cholesteric transition; another candidate for an active chiral liquid crystal might be a solution of DNA fragments interacting with polymerases or other motors [12]. Also, it would be of interest to use the present algorithm to characterise the rheological properties and map out the flow curves of an active liquid crystal under imposed shear. We shall report on such work in future publications. We also hope to report soon on fully three-dimensional simulations of active materials, along the lines pioneered for passive nematics in [40].

We acknowledge EPSRC for support, and are grateful to L. Tubiana for a critical reading of this work.

-
- [1] Y. Hatwalne, S. Ramaswamy, M. Rao, R. A. Simha, *Phys. Rev. Lett.* **92**, 118101 (2004).
 - [2] R.A. Simha, S. Ramaswamy, *Phys. Rev. Lett.* **89**, 058101 (2002).
 - [3] K. Kruse, J. F. Joanny, F. Julicher, J. Prost, K. Sekimoto, *Eur. Phys. J. E* **16**, 5 (2005).
 - [4] K. Kruse *et al.*, *Phys. Rev. Lett.* **92**, 078101 (2004).
 - [5] R. Voituriez, J. F. Joanny, J. Prost, *Phys. Rev. Lett.* **96**, 028102 (2006).
 - [6] T. B. Liverpool, M. C. Marchetti *Phys. Rev. Lett.* **90**, 138102 (2001); *Europhys. Lett.* **69**, 846 (2005); cond-mat/0607285.
 - [7] R. Voituriez, J. F. Joanny, J. Prost, *Europhys. Lett.* **70**, 404 (2005).
 - [8] V. Narayan, N. Menon, S. Ramaswamy, *J. Stat. Mech.: Theory and Experiment* P01005 (2006).
 - [9] I. Llopis, I. Pagonabarraga, *Europhys. Lett.*, **75**, 999 (2006).
 - [10] S. Ramachandran, P. B. S. Kumar, I. Pagonabarraga, *Eur. Phys. J. E* **20**, 151 (2006).
 - [11] D. Bray, *Cell movements: from molecules to motility*, Garland Publishing, New York (2000).
 - [12] P. R. Cook, *Principles of Nuclear Structure and Function*, Wiley, New York (2001).
 - [13] J. van der Gucht, E. Paluch, C. Sykes, *Proc. Natl. Acad. Sci. USA* **102**, 7847 (2005); M. F. Carlier *et al.*, *Bioessays* **25**, 336 (2003); N. J. Burroughs, D. Marenduzzo, *Phys. Rev. Lett.* **98**, 238302 (2007).
 - [14] J. Howard, *Mechanics of Motor Proteins and the Cytoskeleton*, Sinauer Associates, Inc., Sunderland (2001).
 - [15] D. Humphrey *et al.*, *Nature* **416**, 413 (2002).
 - [16] T. Surrey, F. Nedelec, S. Leibler and E. Karsenti, *Science* **292**, 1167 (2001).
 - [17] F. J. Nedelec *et al.*, *Nature* **389**, 305 (1997).
 - [18] P. Kraikivski, R. Lipowsky, J. Kierfeld, *Phys. Rev. Lett.* **96**, 258103 (2006).
 - [19] C. Storm, J.J. Pastore, F.C. MacKintosh, T.C. Lubensky, P.A. Janmey, *Nature* **435**, 191 (2005).
 - [20] D. Marenduzzo, E. Orlandini, M. E. Cates, J. M. Yeomans, *J. Non-Newt. Fluid Mech.*, in press (2007); D. Marenduzzo, E. Orlandini, J. M. Yeomans, *Phys. Rev. Lett.* **98**, 118102 (2007).
 - [21] An active particle “absorbs energy from its surroundings and dissipates it in the process of carrying

- out internal movements, usually resulting in translatory or rotary motion” [1].
- [22] As is conventional [23], we use “phase transition” to refer to a singular dependence of observable quantities on model parameters even in a non-equilibrium system, for which there is no underlying thermodynamic free energy to lead to distinct equilibrium “phases”.
- [23] H. Haken, *Synergetics: An Introduction. Nonequilibrium Phase Transitions and Self-Organization in Physics, Chemistry and Biology*, 3rd rev. enl. ed. New York: Springer-Verlag (1983).
- [24] M. G. Forest, R. H. Zhou, Q. Wang, *Phys. Rev. Lett.* **93**, 088301 (2004).
- [25] B. Chakrabarti, M. Das, C. Dasgupta, S. Ramaswamy, A. K. Sood, *Phys. Rev. Lett.* **92**, 055501 (2004).
- [26] A. Aradian, M.E. Cates, *Europhys. Lett.* **70**, 397 (2005).
- [27] A. N. Morozov, W. van Saarloos, *Phys. Rev. Lett.* **95**, 024501 (2005).
- [28] A. Onuki, *Phase Transition Dynamics*, Cambridge University Press, Cambridge (2002).
- [29] A. Onuki, *J. Phys.: Condens. Matt.* **10**, 49, 11473 (1998).
- [30] M. C. Cross, P. C. Hohenberg, *Rev. Mod. Phys.* **65**, 851 (1993).
- [31] S. C. Glotzer, A. E. Di Marzio, M. Muthukumar, *Phys. Rev. Lett.* **74**, 2034 (1995).
- [32] P.G. de Gennes and J. Prost, *The Physics of Liquid Crystals, 2nd Ed.*, Clarendon Press, Oxford, (1993).
- [33] A.N. Beris and B.J. Edwards, *Thermodynamics of Flowing Systems*, Oxford University Press, Oxford, (1994); A.N. Beris, B.J. Edwards and M. Grmela, *J. Non-Newtonian Fluid Mechanics*, **35** 51 (1990).
- [34] P.D. Olmsted and P.M. Goldbart, *Phys. Rev. A* **46**, 4966 (1992).
- [35] P.D. Olmsted and C.-Y. David Lu, *Phys. Rev. E* **56**, 55 (1997); *ibid.*, **60**, 4397 (1999).
- [36] O. Thoumine, A. Ott, *J. Cell. Sci.* **110**, 2109 (1997).
- [37] J. Uhde, M. Keller, E. Sackmann, A. Parmegiani, E. Frey, *Phys. Rev. Lett.* **93**, 268101 (2004).
- [38] S. Succi, *The Lattice Boltzmann equation*, Oxford University Press (2001).
- [39] C. Denniston, E. Orlandini, J. M. Yeomans, *Phys. Rev. E* **63**, 056702 (2001).
- [40] C. Denniston, D. Marenduzzo, E. Orlandini, J. M. Yeomans, *Phil. Trans. R. Soc. Lond. A* **362**, 1745 (2004).
- [41] D. Marenduzzo, E. Orlandini, J. M. Yeomans, *Europhys. Lett.* **64**, 406 (2003); *J. Chem. Phys.* **121**, 582 (2004).
- [42] D. Marenduzzo, S. Ramaswamy, M. E. Cates, work in progress.
- [43] N. Sulaiman, D. Marenduzzo, J.M. Yeomans, *Phys. Rev. E* **74**, 041708 (2006).

APPENDIX A: COMPARISON OF HYBRID WITH CONVENTIONAL LB CODES

In Fig. 18 we show the director and velocity dynamics at $z = L/4$ (in the geometry of Fig. 3) and in the mid-plane respectively, computed via the hybrid algorithm discussed in this paper and via a full LB algorithm (as described in Refs. [39, 40] for passive nematics and in [20] for the active case). The agreement proves the validity of our hybrid approach. Note that two full LB algorithms are benchmarked against the hybrid code. In one case the double gradient term is entered as a constraint in the second moment, in the other its derivative is entered as a body

force (this second procedure guarantees that no spurious velocities are found in steady state, see e.g. Ref. [43]). It can be seen that the LB treatment with the double gradient terms entered in the second moment constraint leads to a small deviation at intermediate times. This we interpret as a discretisation error, as this method in 2D is known (for conventional i.e. passive liquid crystals) to lead to discretization errors causing small spurious velocities even in the steady state [43].

APPENDIX B: “ERICKSEN-LESLIE” LIMIT OF THE ORDER PARAMETER EVOLUTION EQUATION

In this Appendix we map the order parameter evolution equation used in this work, Eq. 5, onto the analogous equation used in Ref. [7], by taking the limit of a uniaxial liquid crystal with spatially uniform and temporally constant magnitude of ordering q . In this way we will recover Eqs. 28 and 29.

To this end let us first write the \mathbf{Q} evolution equation (5) for \mathbf{H} . This gives, formally,

$$\Gamma\mathbf{H} = (\partial_t + \mathbf{u} \cdot \nabla)\mathbf{Q} - \mathbf{S}(\mathbf{W}, \mathbf{Q}) - \lambda\mathbf{Q}. \quad (\text{B1})$$

By considering the uniaxial expression for \mathbf{Q} (see Eq. 11) we obtain

$$\begin{aligned} \Gamma H_{\beta\mu} = & (\partial_t q)n_\beta n_\mu - \frac{\delta_{\beta\mu}}{3}\partial_t q + (u_\gamma \partial_\gamma q)n_\beta n_\mu - \frac{\delta_{\beta\mu}}{3}(u_\gamma \partial_\gamma q)\delta_{\beta\mu} \\ & + q(\partial_t n_\beta)n_\mu + qn_\beta(\partial_t n_\mu) + q(u_\gamma \partial_\gamma n_\beta)n_\mu + qn_\beta(u_\gamma \partial_\gamma n_\mu) \\ & - \lambda q n_\beta n_\mu + \lambda q \frac{\delta_{\beta\mu}}{3} + \frac{2}{3}\xi(q-1)D_{\beta\mu} \\ & - \xi q(D_{\beta\gamma}n_\gamma n_\mu + n_\beta n_\gamma D_{\gamma\mu}) - q(\Omega_{\beta\gamma}n_\gamma n_\mu - n_\beta n_\gamma \Omega_{\gamma\mu}) \\ & + 2q\xi n_\beta n_\mu \text{Tr}(\mathbf{Q}\mathbf{W}) - \frac{2}{3}\xi(q-1)\text{Tr}(\mathbf{Q}\mathbf{W}). \end{aligned} \quad (\text{B2})$$

As can be easily checked, one can substitute \mathbf{W} with \mathbf{D} in (B2). As we have assumed that q does not depend on t and \vec{r} , we obtain:

$$\begin{aligned} \Gamma H_{\beta\mu} = & q(n_\mu N_\beta + n_\beta N_\mu) - q\xi(D_{\beta\gamma}n_\gamma n_\mu + n_\beta n_\gamma D_{\gamma\mu}) - \lambda q \left(n_\beta n_\mu - \frac{\delta_{\beta\mu}}{3} \right) \\ & + \frac{2}{3}(q-1)\xi D_{\beta\mu} + \frac{1}{2}q^2\xi n_\beta n_\mu D_{\gamma\nu}n_\nu n_\gamma + \frac{2}{3}q(1-q)\xi\delta_{\beta\mu}D_{\gamma\nu}n_\nu n_\gamma \end{aligned} \quad (\text{B3})$$

where N_β, N_μ are co-rotational derivatives defined as,

$$\begin{aligned} N_\beta = & \partial_t n_\beta + u_\gamma \partial_\gamma n_\beta + \Omega_{\beta\gamma}n_\gamma \\ = & \partial_t n_\beta + u_\gamma \partial_\gamma n_\beta - (\boldsymbol{\omega} \times \mathbf{n})_\beta \end{aligned} \quad (\text{B4})$$

and $\boldsymbol{\omega} = \nabla \times \mathbf{u}/2$. In order to write the evolution equation (B3) in a form that resembles the one introduced in [7] we note first that, by the chain rule,

$$\begin{aligned} h_\mu = & -\frac{\delta\mathcal{F}}{\delta n_\mu} = -\frac{\delta\mathcal{F}}{\delta Q_{\alpha\beta}} \frac{\partial Q_{\alpha\beta}}{\partial n_\mu} \\ = & H_{\alpha\beta}q(n_\beta \delta_{\alpha\mu} + n_\alpha \delta_{\beta\mu}) \\ = & q(n_\beta H_{\beta\mu} + n_\alpha H_{\alpha\mu}) = 2q(n_\beta H_{\beta\mu}). \end{aligned} \quad (\text{B5})$$

If we now multiply (on the left) both members of Eq. (B3) by n_β and we use the constraint $n_\beta n_\beta = 1$ we obtain after some algebra,

$$\Gamma h_\mu / 2q = qN_\mu - \frac{1}{3}(q+2)\xi n_\gamma D_{\gamma\mu} - \frac{2}{3}\lambda q n_\mu \quad (\text{B6})$$

where we have omitted terms $O(n^3)$. Clearly, if $\lambda = 0$, Eq. (B6) reduces to the usual Ericksen-Leslie equation for the director field, namely [32]

$$h_\mu = \gamma_1 N_\mu + \gamma_2 n_\alpha D_{\alpha\mu} \quad (\text{B7})$$

where

$$\gamma_1 = \frac{2q^2}{\Gamma}, \quad (\text{B8})$$

$$\gamma_2 = -\frac{2q}{3\Gamma}(q+2)\xi. \quad (\text{B9})$$

If, on the other hand, the active term $\lambda \neq 0$ we have

$$N_\mu = \frac{\Gamma}{2q^2} h_\mu + \frac{1}{3} \frac{(q+2)}{q} \xi n_\gamma D_{\gamma\mu}. \quad (\text{B10})$$

Note that terms proportional to n_μ drop out of the equations in this mapping. Indeed they contribute a component of the molecular field parallel to n_μ , which would tend to increase the magnitude of the director field q . This is prevented by the Lagrange multiplier which appears in the vectorial ‘‘Ericksen-Leslie’’ model (to maintain constant q). As a result such terms simply change the relationship between the Lagrange multiplier and the magnitude of order and not the structure of the director field equation. By comparing Eq. (B10) with Eq. (3) of [7] (there $Dn_\mu/Dt = N_\mu$) we then obtain the relations listed in Eqs. (28) and (29) in the text.

APPENDIX C: ‘‘ERICKSEN-LESLIE’’ LIMIT OF THE NAVIER-STOKES EQUATION

In this Appendix we work out the details of the mapping between the Navier-Stokes equation in our tensorial model in the uniaxial limit of constant q , and the momentum balance equation used in the ‘‘Ericksen-Leslie’’ version of Ref. [7], which was reported in Section III B in the text. To this end, we need to write the total stress tensor $\Pi_{\alpha\beta} = \Pi_{\alpha\beta}^{passive} + \Pi_{\alpha\beta}^{active}$ in terms of the molecular and director fields, h_μ and n_μ respectively, which are used in director field based models. As in Appendix B we write $Q_{\alpha\beta}$ in uniaxial form i.e $\mathbf{Q} = q(\mathbf{P} - \mathbf{I}/3)$ where $P_{\alpha\beta} = n_\alpha n_\beta$. Note that $\mathbf{P}^2 = \mathbf{P}$ and $Tr(\mathbf{P}) = 1$ and recall that the Ericksen-Leslie expression for the total stress is:

$$\begin{aligned} \sigma_{\alpha\beta}^{EL} &= \alpha_1 n_\alpha n_\beta n_\mu n_\rho D_{\mu\rho} + \alpha_4 D_{\alpha\beta} + \alpha_5 n_\beta n_\mu D_{\mu\alpha} \\ &\quad + \alpha_6 n_\alpha n_\mu D_{\mu\beta} + \alpha_2 n_\beta N_\alpha + \alpha_3 n_\alpha N_\beta. \end{aligned} \quad (\text{C1})$$

We first consider the anti-symmetric part of the passive stress tensor in the tensorial model, namely:

$$\begin{aligned} \tau_{\alpha\beta} &= \mathbf{Q} \cdot \mathbf{H} - \mathbf{H} \cdot \mathbf{Q} \\ &= q(\mathbf{P} \cdot \mathbf{H} - \mathbf{H} \cdot \mathbf{P}). \end{aligned} \quad (\text{C2})$$

Multiplying to the left the expression (B3) for $H_{\alpha\gamma}$ by $P_{\alpha\gamma} = n_\alpha n_\gamma$ and to the right by $n_\gamma n_\beta$, gives, after some algebra

$$\begin{aligned}\Gamma\tau_{\alpha\beta} &= q\Gamma(n_\alpha n_\gamma H_{\gamma\beta} - H_{\alpha\gamma} n_\gamma n_\beta) \\ &= \left[q^2(n_\alpha N_\beta - N_\alpha n_\beta) - \frac{\xi q}{3}(q+2)(n_\alpha n_\gamma D_{\gamma\beta} - D_{\alpha\gamma} n_\gamma n_\beta) \right].\end{aligned}\quad (\text{C3})$$

Eq. (C3) may now be compared to the antisymmetric part of Eq. (C2), to give

$$\alpha_3 - \alpha_2 = \frac{2q^2}{\Gamma} = \gamma_1, \quad (\text{C4})$$

$$\alpha_6 - \alpha_5 = -\frac{2}{3}q\xi\left(\frac{q+2}{\Gamma}\right) = \gamma_2 \quad (\text{C5})$$

where the equalities with γ_1, γ_2 come from comparison with Eq. (B9). We may slightly rewrite the antisymmetric term (C3) in a form that is closer to the one used in [7]. This can be done by substituting the expression for N_μ written in terms of the molecular field

$$N_\mu = \frac{h_\mu}{\gamma_1} - \frac{\gamma_2}{\gamma_1} n_\sigma D_{\sigma\mu} \quad (\text{C6})$$

into (C3). This gives

$$\Gamma\tau_{\alpha\beta} = \frac{q^2}{\gamma_1} (n_\alpha h_\beta - h_\alpha n_\beta) + q^2 \frac{\gamma_2}{\gamma_1} (n_\sigma D_{\sigma\alpha} n_\beta - n_\alpha n_\sigma D_{\sigma\beta}) - \frac{\xi q}{3}(q+2)(n_\alpha n_\sigma D_{\sigma\beta} - D_{\alpha\sigma} n_\sigma n_\beta). \quad (\text{C7})$$

Hence the expression for $\tau_{\alpha\beta}$ simplifies to

$$\tau_{\alpha\beta} = \frac{q^2}{\Gamma\gamma_1} (n_\alpha h_\beta - h_\alpha n_\beta) \quad (\text{C8})$$

which is the antisymmetric term in the director field treatment of Ref. [7] (see eq. (2) of [7]).

We now turn to the symmetric part of the total stress tensor (excluding the active contribution and the double gradient term):

$$\begin{aligned}\sigma_{\alpha\beta} &= -P_0\delta_{\alpha\beta} + 2\xi(Q_{\alpha\beta} + \frac{1}{3}\delta_{\alpha\beta})Q_{\gamma\epsilon}H_{\gamma\epsilon} \\ &\quad - \xi H_{\alpha\gamma}(Q_{\gamma\beta} + \frac{1}{3}\delta_{\gamma\beta}) - \xi(Q_{\alpha\gamma} + \frac{1}{3}\delta_{\alpha\gamma})H_{\gamma\beta}\end{aligned}\quad (\text{C9})$$

The active contribution is:

$$\Pi_{\alpha\beta}^{\text{active}} = -\zeta q n_\alpha n_\beta + \zeta \frac{q}{3} \delta_{\alpha\beta}. \quad (\text{C10})$$

Note that the double gradient term $-\partial_\alpha Q_{\gamma\nu} \frac{\delta\mathcal{F}}{\delta\partial_\beta Q_{\gamma\nu}}$ is analogous to the director field term $-\partial_\alpha n_\nu \frac{\delta\mathcal{F}}{\delta\partial_\beta n_\nu}$, which is not included in Eq. (C2) hence not considered hereafter.

By using Eq. (B3) for \mathbf{H} , after some algebra, one obtains the complete expression for $\sigma_{\alpha\beta}$ as

$$\begin{aligned}\sigma_{\alpha\beta} &= -\frac{q\xi}{3\Gamma}(q+2)(n_\beta N_\alpha + n_\alpha N_\beta) + \frac{\xi^2 q}{3\Gamma}(4-q)(D_{\alpha\gamma} n_\gamma n_\beta + n_\alpha n_\gamma D_{\gamma\beta}) \\ &+ \frac{4}{9\Gamma}(q-1)^2 \xi D_{\alpha\beta} + \frac{2}{3\Gamma} q^2 \xi^2 (4q^2 - 4q - 3) n_\alpha n_\beta D_{\gamma\nu} n_\nu n_\gamma \\ &+ \frac{q\xi^2}{\Gamma}(4 - 7q - 8q^2 + 8q^3) \delta_{\alpha\beta} D_{\gamma\nu} n_\nu n_\gamma\end{aligned}$$

The first term of the right hand side of Eq. (C11) can be usefully rewritten (for comparison with the equation in [7]) by using (C6) to write N_μ in terms of h_μ .

$$\begin{aligned}-q\xi/3(q+2)(n_\beta N_\alpha + n_\alpha N_\beta) &= -q\xi/3(q+2) \left(n_\beta \frac{h_\alpha}{\gamma_1} - n_\beta \frac{\gamma_2}{\gamma_1} n_\sigma D_{\sigma\alpha} + n_\alpha \frac{h_\beta}{\gamma_1} - n_\alpha \frac{\gamma_2}{\gamma_1} n_\sigma D_{\sigma\beta} \right) \\ &= \frac{\nu_{EL}\Gamma}{2} (n_\beta h_\alpha + n_\alpha h_\beta) - \frac{\nu_{EL}\Gamma\gamma_2}{2} (n_\beta n_\sigma D_{\sigma\alpha} + n_\alpha n_\sigma D_{\sigma\beta})\end{aligned}\quad (\text{C11})$$

where in the last line we have used Eq. (29).

The Navier Stokes equation in the Stokes regime is

$$\eta\partial_\beta(\partial_\alpha u_\beta + \partial_\beta u_\alpha) = 2\partial_\beta\eta D_{\alpha\beta} = -\partial_\beta(\Pi_{\alpha\beta}).\quad (\text{C12})$$

$-\Pi_{\alpha\beta}$ can equivalently be rewritten as

$$\begin{aligned}-\Pi_{\alpha\beta} &= -\frac{\nu_{EL}}{2} (n_\beta h_\alpha + n_\alpha h_\beta) + \frac{4\xi^2}{9\Gamma}(q-1)^2 (D_{\alpha\sigma} n_\sigma n_\beta + n_\alpha n_\sigma D_{\sigma\beta}) \\ &- \frac{4}{9\Gamma}(q-1)^2 \xi^2 D_{\alpha\beta} - \frac{2}{3\Gamma} q^2 \xi^2 (4q^2 - 4q - 3) n_\alpha n_\beta D_{\gamma\nu} n_\nu n_\gamma \\ &- \frac{q\xi^2}{\Gamma}(4 - 7q - 8q^2 + 8q^3) \delta_{\alpha\beta} D_{\gamma\nu} n_\nu n_\gamma \\ &+ \zeta q n_\alpha n_\beta - \zeta \frac{q}{3} \delta_{\alpha\beta} \\ &- \frac{q^2}{\Gamma\gamma_1} (n_\alpha h_\beta - h_\alpha n_\beta).\end{aligned}\quad (\text{C13})$$

If $\lambda = \zeta = 0$, i.e. for passive liquid crystals, Eq. (C11) gives the symmetric part of the Beris-Edwards stress (ignoring the distortion stress) and this, together with Eq. (C3) gives the Leslie coefficients which are listed in Section III B (Eqs. 31–36).

In Eq. (C13) the term proportional to $D_{\alpha\beta}$ may be added to the left hand side in Eq. C12 to renormalise the apparent viscosity, while the rest of it may be rewritten as

$$\begin{aligned}&- \frac{\nu_{EL}}{2} (n_\beta h_\alpha + n_\alpha h_\beta) + \frac{4\xi^2}{9\Gamma}(q-1)^2 (D_{\alpha\sigma} n_\sigma n_\beta + n_\alpha n_\sigma D_{\sigma\beta}) \\ &- \frac{2}{3\Gamma} q^2 \xi^2 (4q^2 - 4q - 3) n_\alpha n_\beta D_{\gamma\nu} n_\nu n_\gamma \\ &- \frac{q\xi^2}{\Gamma}(4 - 7q - 8q^2 + 8q^3) \delta_{\alpha\beta} D_{\gamma\nu} n_\nu n_\gamma \\ &+ \zeta q n_\alpha n_\beta - \zeta \frac{q}{3} \delta_{\alpha\beta} \\ &- \frac{1}{2} (n_\alpha h_\beta - h_\alpha n_\beta)\end{aligned}\quad (\text{C14})$$

where for the last term we have used relation (B9). By comparing our equation with the one in [7] we then get Eqs. (40), (29) in the text.

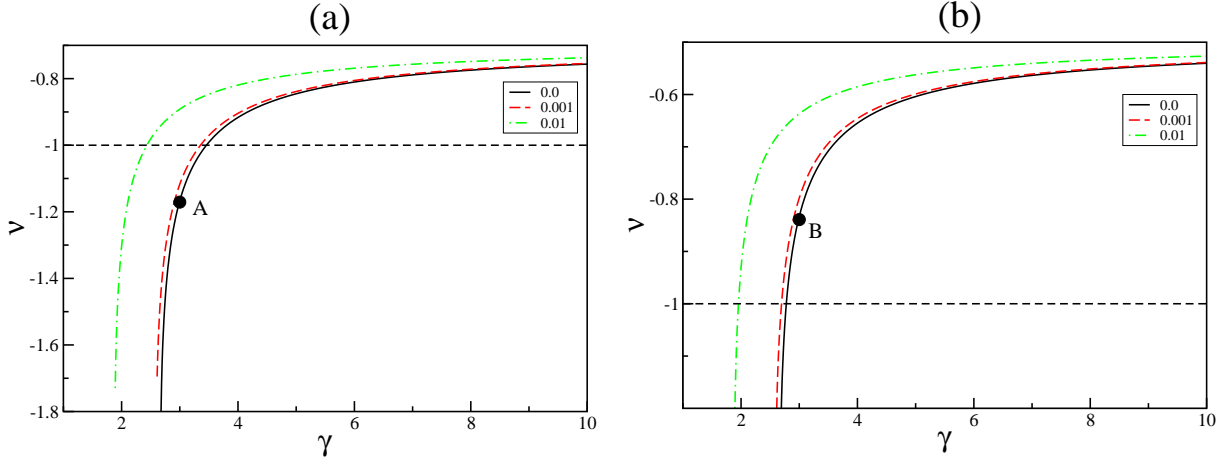


FIG. 1: Plot of the γ dependence of ν_{EL} ; panels in (a) and (b) have $\chi = 0.7, 0.5$ respectively. Within each panel different curves refer to different activity levels λ (see legend). Note that for $\xi = 0.5$, flow tumbling ($|\nu_{EL}| < 1$) is expected throughout the nematic phase. Points A and B represent numerical examples described below.

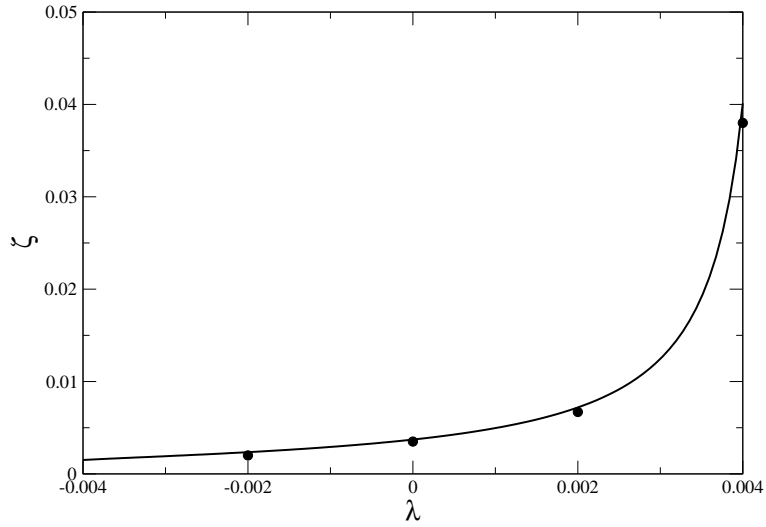


FIG. 2: Phase boundary for $L = 49$ in the (λ, ζ) plane for $\gamma = 3.0$, $\tau_f = 1$ and $\xi = 0.7$. Four points found numerically from our HLB simulations are also shown (filled circles).

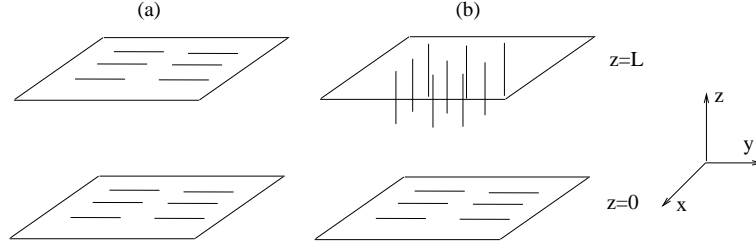


FIG. 3: Geometry used for the calculations described in the text. The active gel is sandwiched between two infinite plates, parallel to the xy plane, lying at $z = 0$ and $z = L$. We consider (a) normal anchoring and (b) conflicting anchoring. (The latter would correspond to a hybrid aligned nematic (HAN) cell for a passive liquid crystal material.)

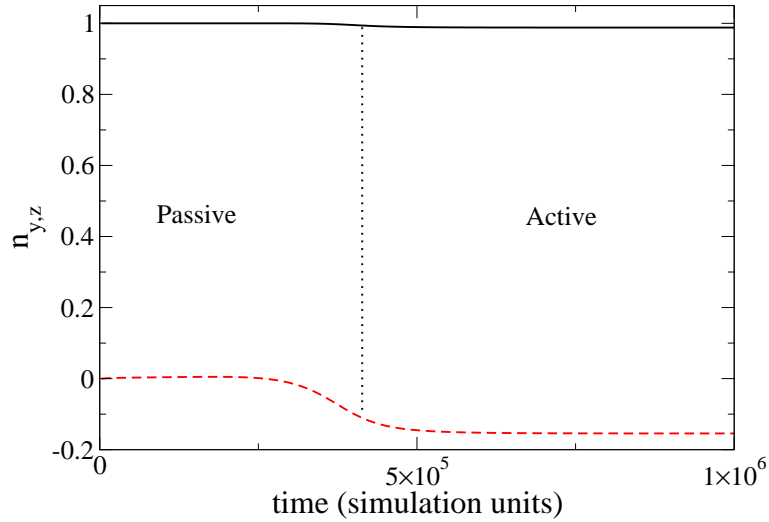


FIG. 4: Time evolution of the components of the polarization field n_y (upper) and n_z (lower), at $z = L/4$. Parameters are $L = 100$, $\zeta = 0.005$, $\lambda = 0$, $\gamma = 3$, $\tau_f = 2.5$ and $\xi = 0.7$ (flow aligning regime). At the bounding plates, the field is strongly anchored along the y direction (homogeneous anchoring).

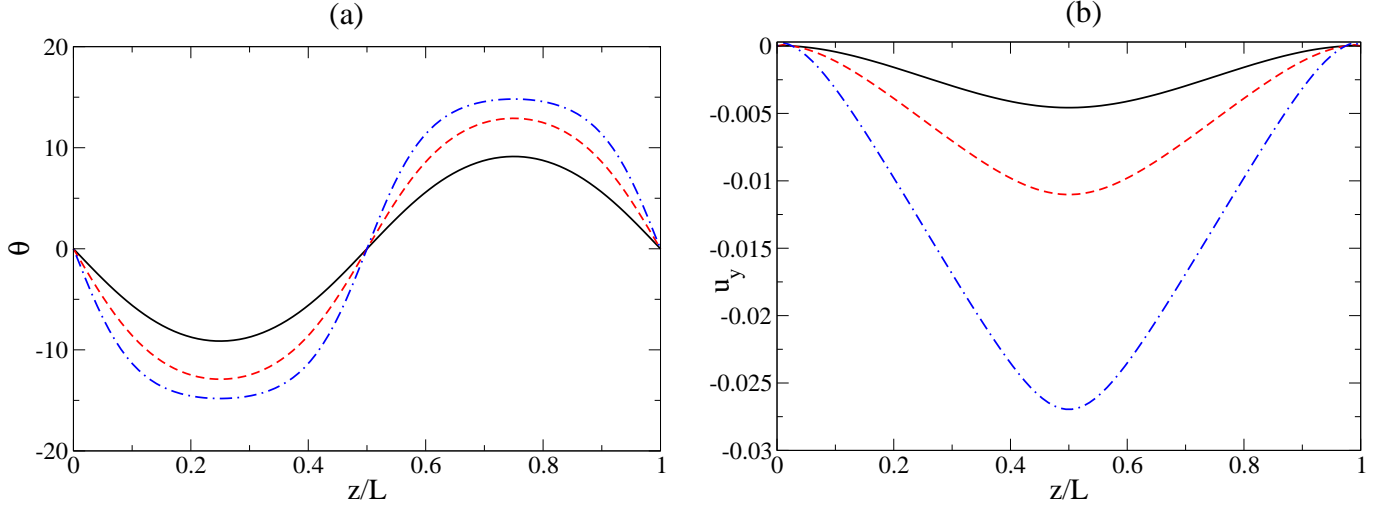


FIG. 5: Profiles of director orientation angle (a) and velocity field (b; in lattice units) at steady state for different values of ζ in a flow-aligning active liquid crystal sample with $L = 100$ (other parameters as specified in the text). Solid, dashed and dot-dashed curves correspond to $\zeta = 0.003, 0.005, 0.01$ respectively. The transition to the active phase occurs at $\zeta = \zeta_c \simeq 0.002$. The flow is bistable: reversing the sign of θ and u_y together creates an alternative steady-state solution.

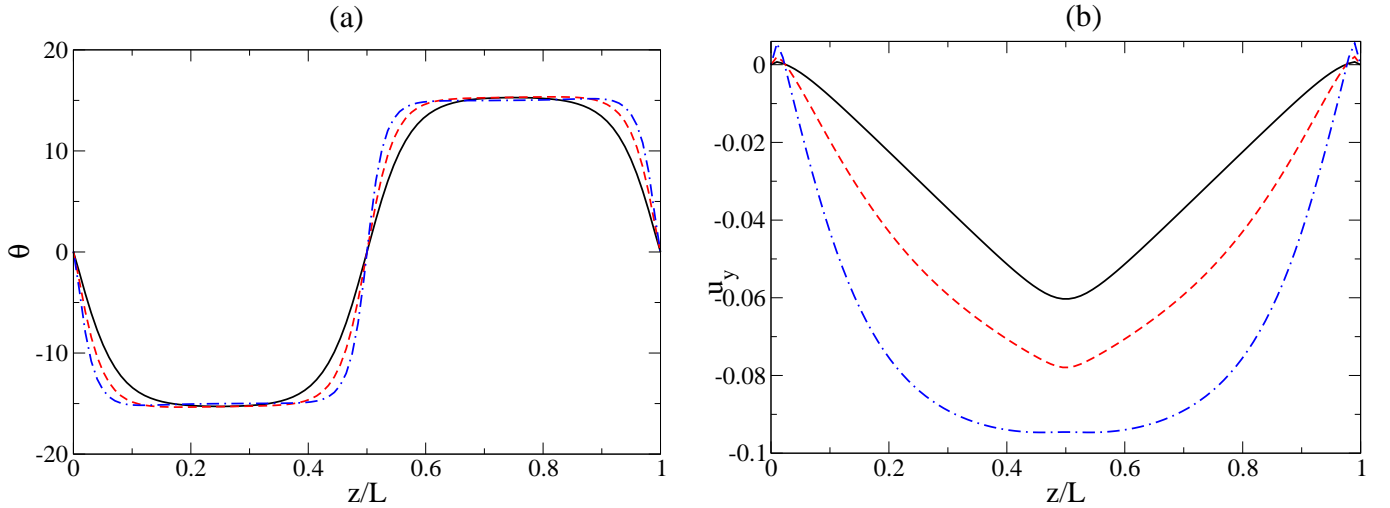


FIG. 6: Profiles of director orientation (a) and velocity field (b, lattice units) at steady state for different values of ζ in a flow-aligning active liquid crystal sample with $L = 100$ (other parameters as specified in the text). Solid, dashed and dot-dashed curves correspond to $\zeta = 0.02, 0.04, 0.08$ respectively. All solutions are bistable (see text).

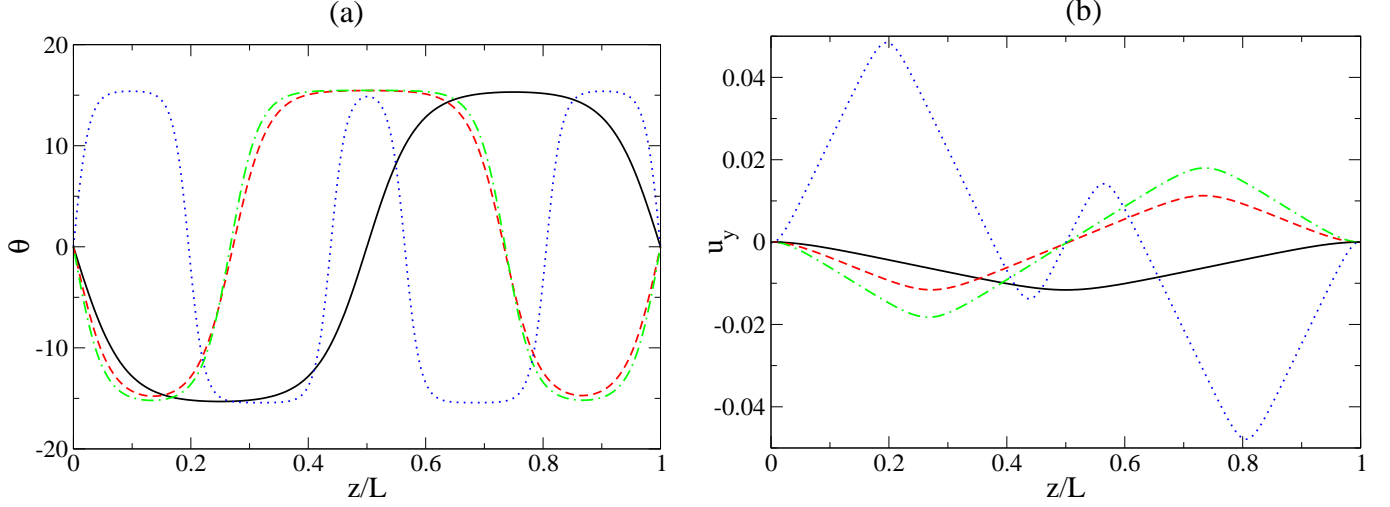


FIG. 7: Profiles of director orientation (a) and velocity field (b, lattice units) at steady state for different values of ζ in a flow-aligning active liquid crystal sample with $L = 400$ (other parameters as specified in the text). Solid, dashed, dot-dashed and dotted lines correspond to $\zeta = 0.001, 0.002, 0.003, 0.01$ respectively.

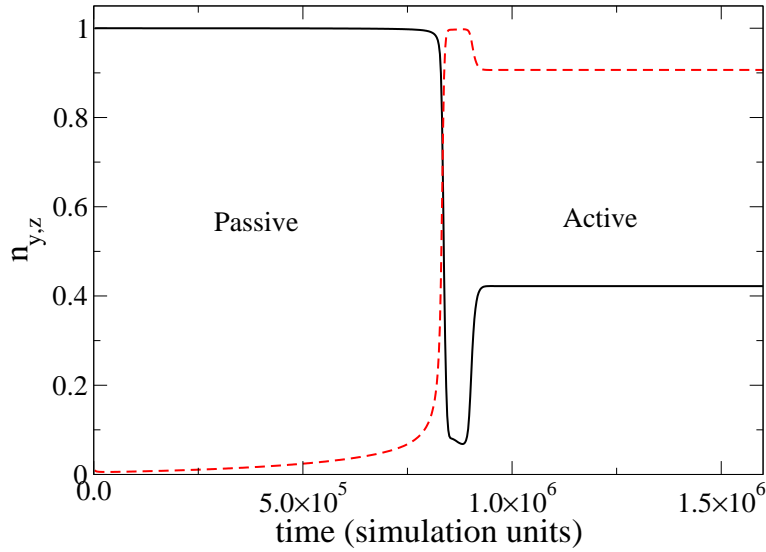


FIG. 8: Time evolution of the components of the polarization field at $z = L/2$ for the flow tumbling case ($\xi = 0.5$). Other parameters are $L = 100$, $\zeta = -0.0025$, $\lambda = 0$, $A_0 = 0.1$, and $K = 0.04$; the transition as predicted by Eq. 42 is at $\zeta = \zeta^* \simeq -0.0022$. The director field is strongly anchored along the y direction (homogeneous anchoring).

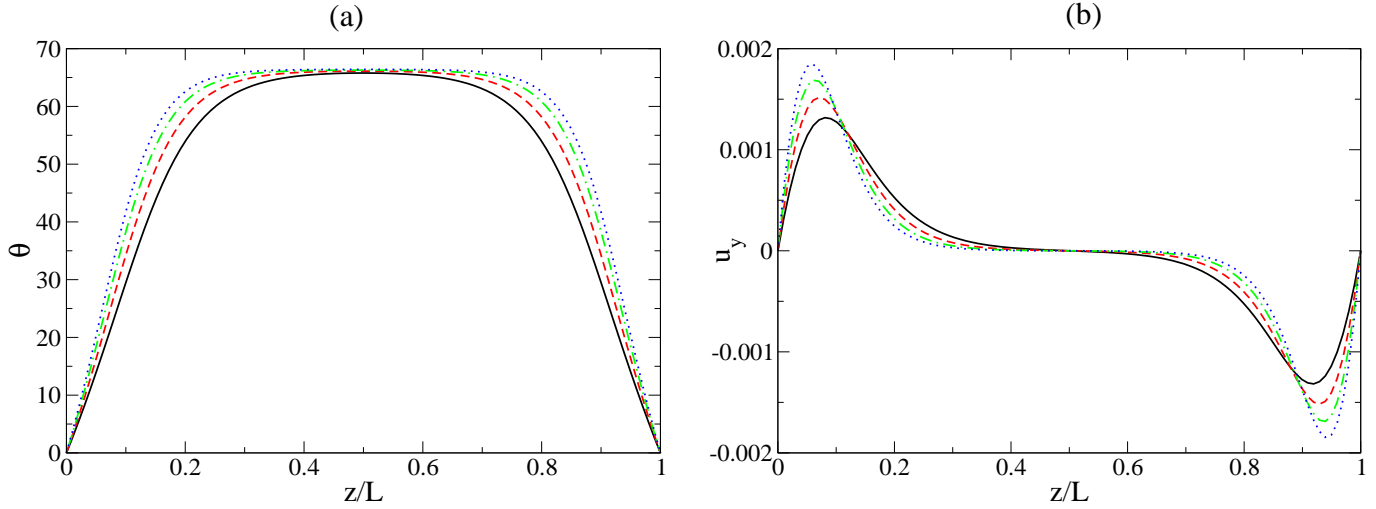


FIG. 9: Polarization angle (a) and velocity field (b) profiles for flow-tumbling active liquid crystals, with $\zeta = -0.003$ (solid black line), -0.004 (dashed red line), -0.005 (dot-dashed green line), and -0.006 (dotted blue line). The transition between the passive and the active phase is attained at $\zeta = \zeta_c \simeq -0.002$ (see also Eq. 42).

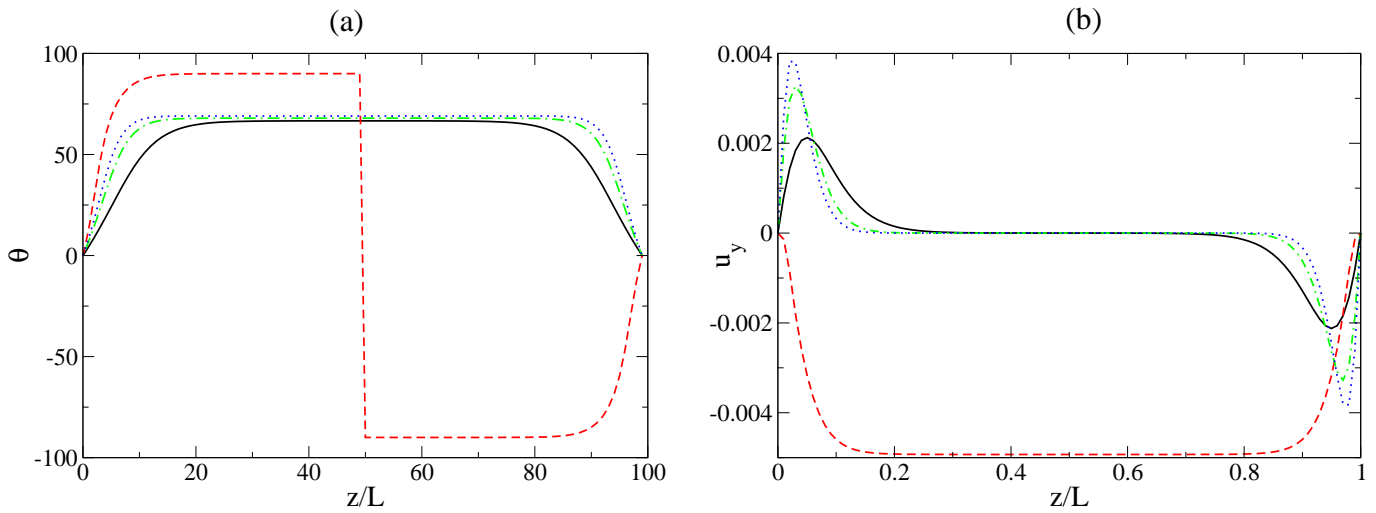


FIG. 10: Polarisation angle (a) and velocity (b) profiles for flow-tumbling active liquid crystals deep in the active phase. Curves correspond to $\zeta = -0.008$ (solid black line), -0.01 (dashed red line), -0.02 (dot-dashed green line), and -0.03 (dotted blue line).

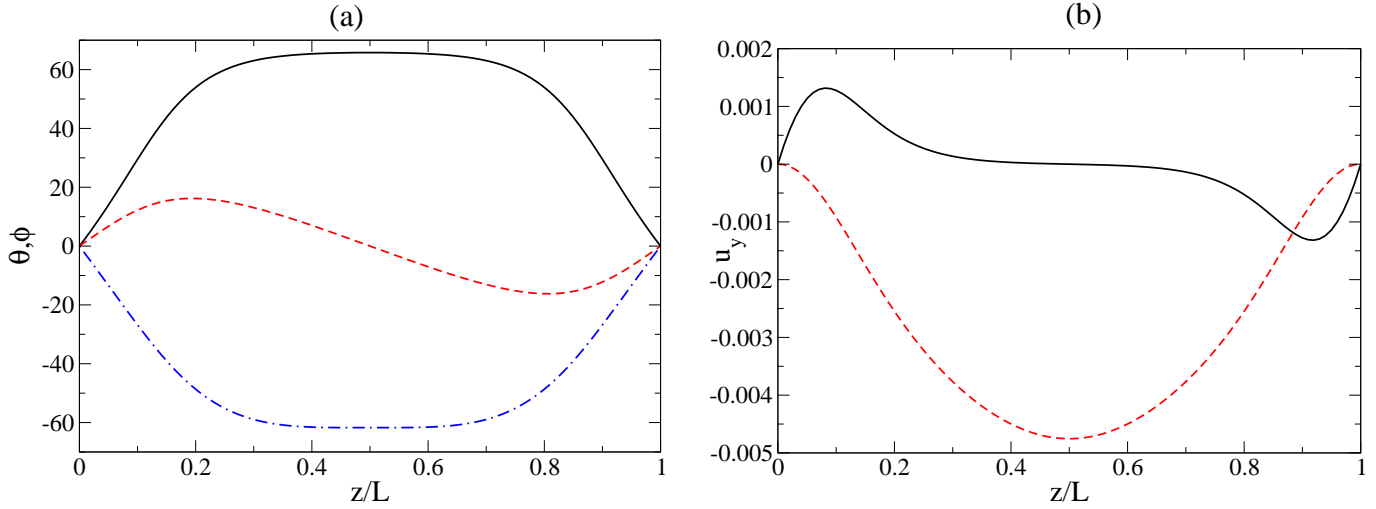


FIG. 11: Profiles of director orientation (a) and velocity (b) for two different steady state solutions found for contractile tumbling liquid crystals in the active phase ($\zeta = -0.003$) in the geometry of Fig. 3a), starting with two different initial conditions. In (a) the solid and the dot-dashed line refer to the two different polarisation angles, while the long dashed line refers to the ϕ angle between the projection of the director angle onto the xy plane and the positive x axis. Initial conditions are given in the text.

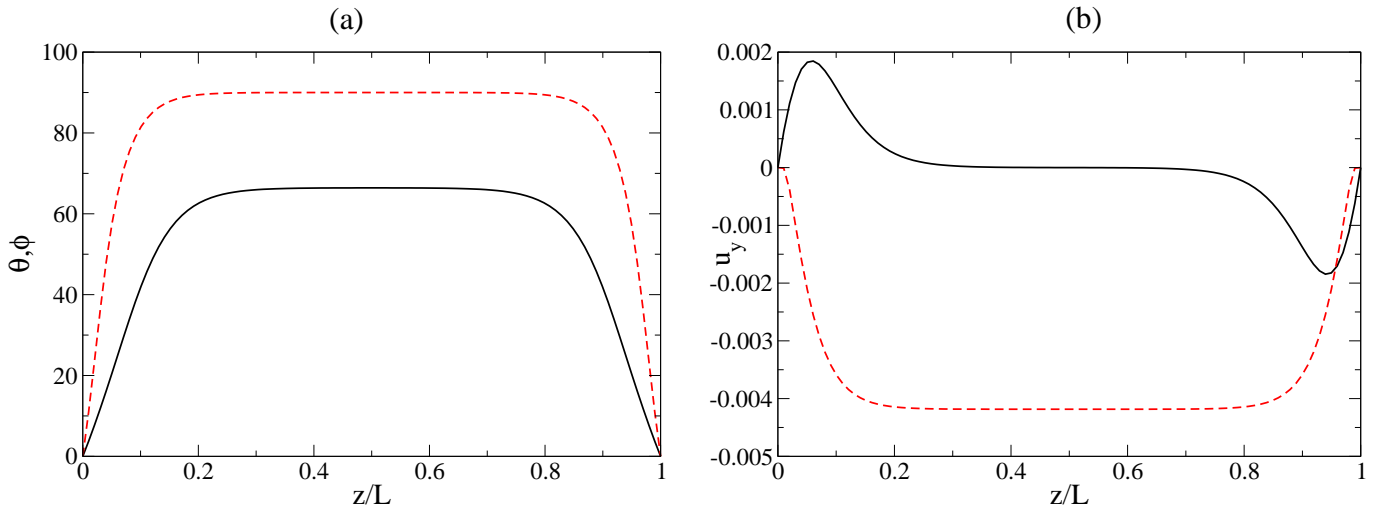


FIG. 12: Profiles of director orientation (a) and velocity (b) for two different steady state solutions found for contractile tumbling liquid crystals in the active phase ($\zeta = -0.006$) in the geometry of Fig. 3a). Initial conditions are given in the text.

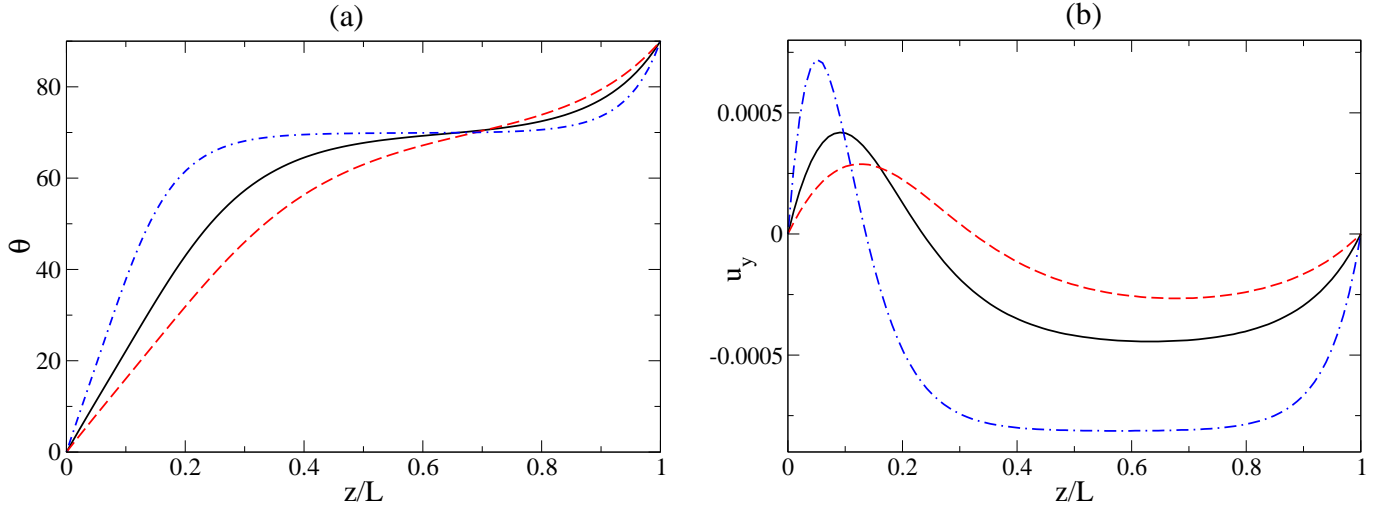


FIG. 13: Profiles of director orientation (a) and velocity (b) for flow-aligning contractile active liquid crystals in a HAN geometry. Curves correspond to $\zeta = -0.001$ (solid black line), -0.0005 (dashed red line), -0.003 (dot-dashed blue line).

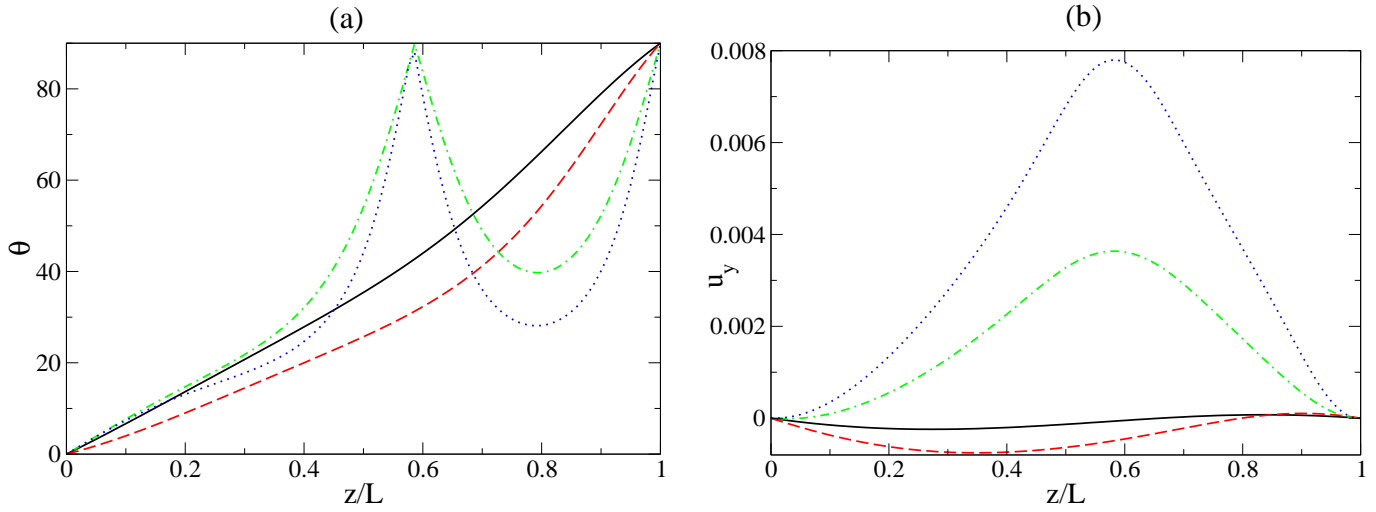


FIG. 14: Profiles of director orientation (a) and velocity (b) for flow-aligning extensile active liquid crystals in a HAN geometry. Curves correspond to $\zeta = -0.001$ (solid black line), -0.0005 (dashed red line), -0.003 (dot-dashed blue line).

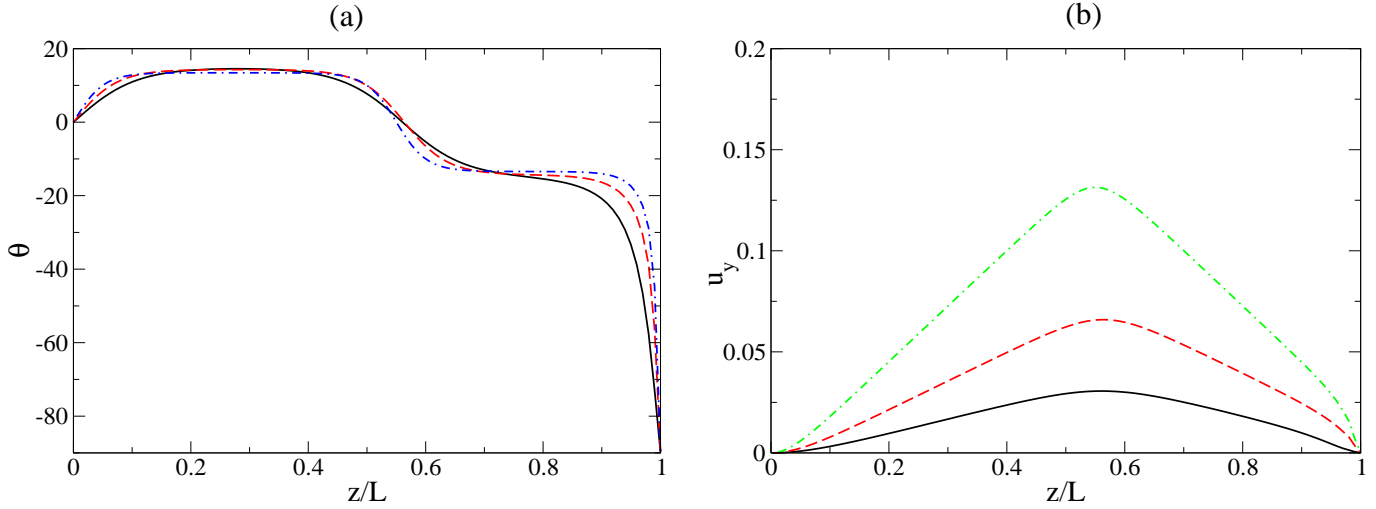


FIG. 15: Profiles for director orientation (a) and velocity (b) for flow-aligning extensile active liquid crystals in a HAN geometry. Curves correspond to $\zeta = -0.001$ (solid black line), -0.0005 (dashed red line), -0.003 (dot-dashed blue line).

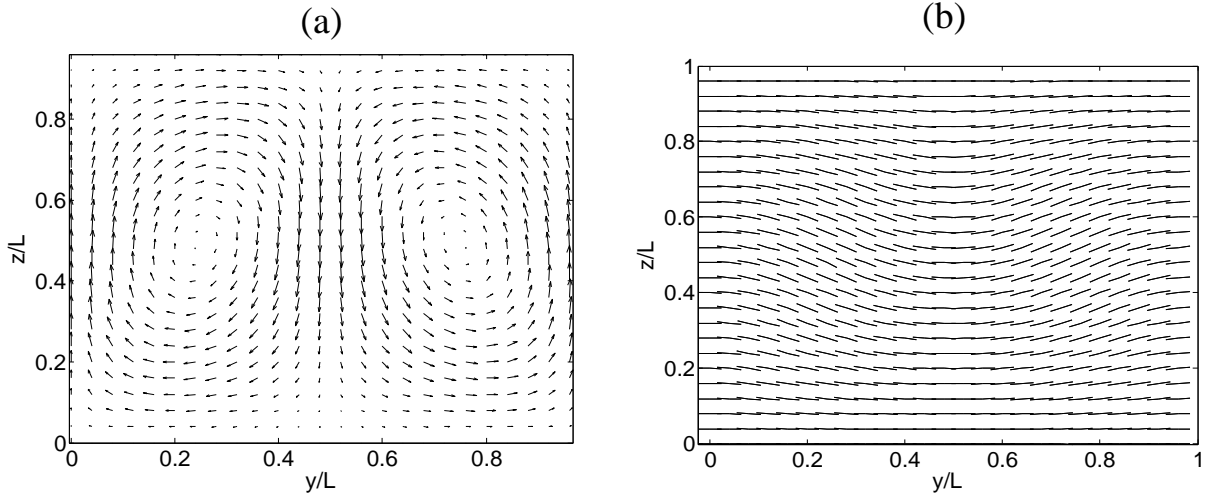


FIG. 16: Maps of velocity field (a) and director field (b) in steady state for an active aligning liquid crystal with $\zeta = 0.001$ (extensile), simulated on a two-dimensional $L = 100 \times L = 100$ grid.

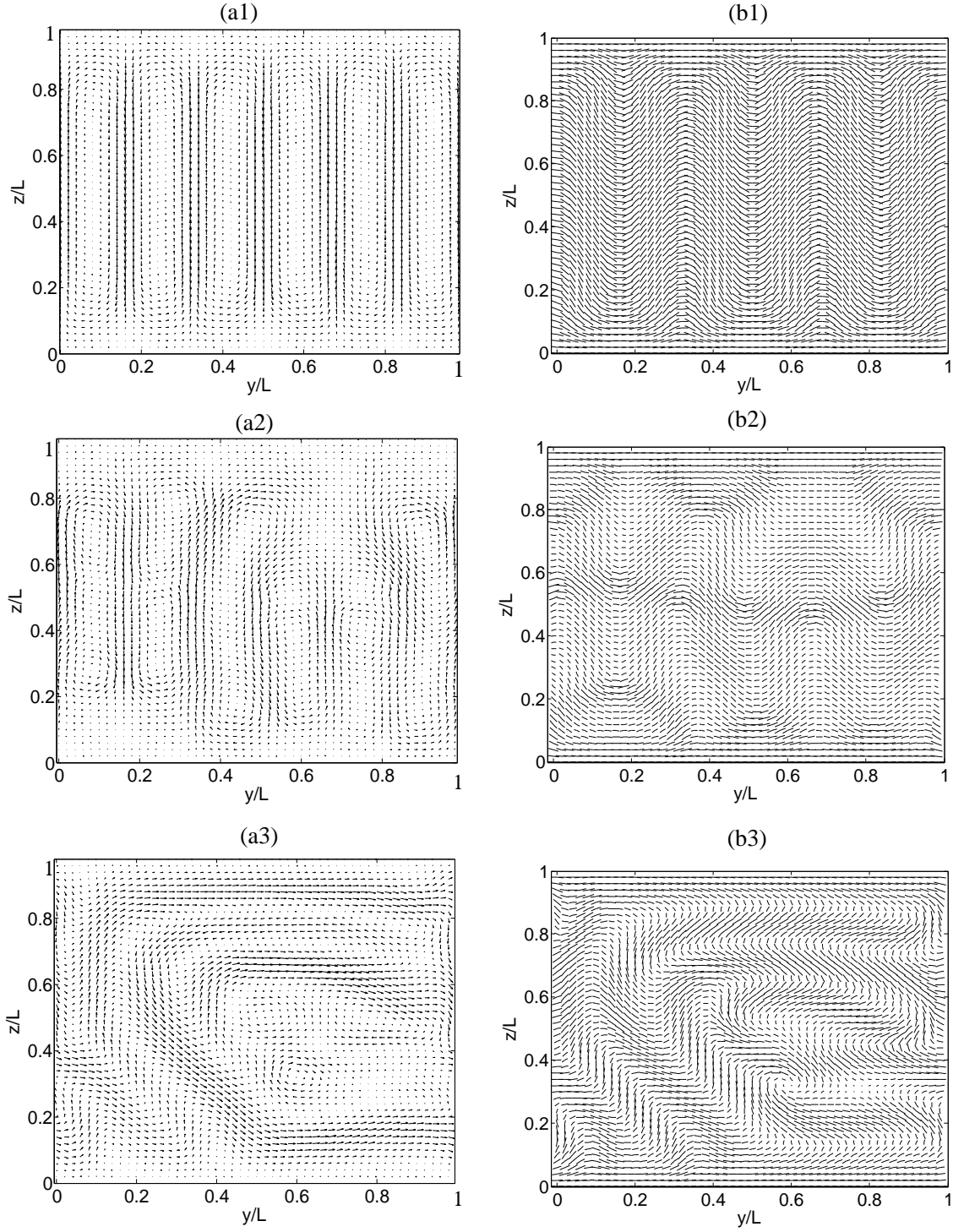


FIG. 17: Maps of velocity field (a1-a3) and director field (b1-b3) for an active aligning liquid crystal with $\zeta = 0.01$ (extensile), simulated on a two-dimensional $L = 100 \times L = 100$ grid. The three rows correspond to the configurations after 10^4 , 3×10^4 , 10^5 lattice Boltzmann steps respectively.

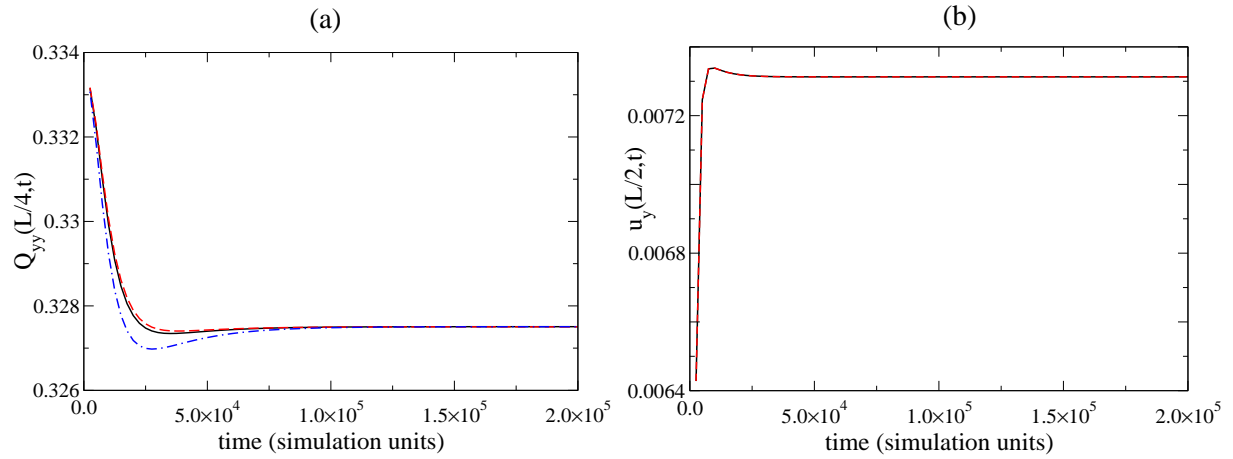


FIG. 18: Time evolution of Q_{yy} at $z = L/4$ (a) and of u_y in the mid-plane (b), as predicted by our hybrid LB treatment (solid black lines), and by two types of full LB treatment (dashed red lines, with the double gradient terms entered in the first moment constraint, to avoid spurious velocities at equilibrium; and dot-dashed blue lines, with the double gradient term entered in the second moment constraint).